

AD-A183 076

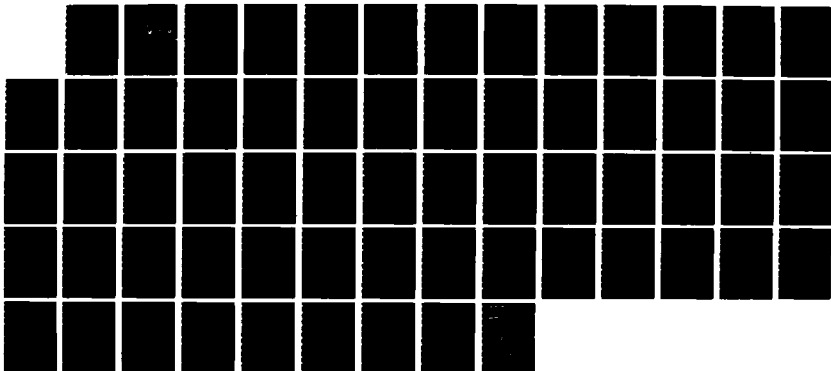
AMBIENT SCATTERING FROM RING-SYMMETRIC SPACECRAFT
EXHAUST PLUME(U) FALCOVITZ (JOSEPH) HAIFA (ISRAEL)
J FALCOVITZ APR 87 NPS-72-87-001CR N00228-87-C-3046

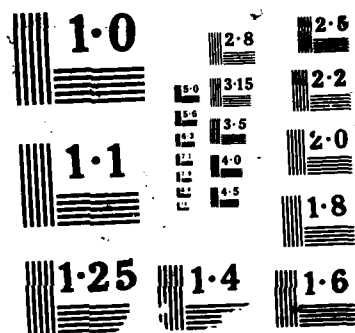
1/1

UNCLASSIFIED

F/G 20/4

NL





NPS72-87-003CR

DTIC FILE COPY

NAVAL POSTGRADUATE SCHOOL

Monterey, California



DTIC
ELECTE
AUG 1 1 1987
S D

CONTRACTOR REPORT

AMBIENT SCATTERING FROM RING-SYMMETRIC
SPACECRAFT EXHAUST PLUME

by

Joseph Falcovitz

April 1987

Approved for public release; distribution unlimited.

Prepared for: Strategic Defense Initiative Office
The Pentagon
Washington, DC 20301-7100

NAVAL POSTGRADUATE SCHOOL
Monterey, California

RADM R. C. Austin
Superintendent

D. A. Schradly
Provost

The work reported herein was performed for the Naval Postgraduate School by Dr. Joseph Falcovitz under contract N00228-87-C-3046. The work presented in this report is in support of "Rarefied Gas Dynamics of Laser Exhaust Plume" sponsored by the Strategic Defense Initiative Office/Directed Energy Office. This is the final report for that contract. The work provides information concerning scattering of exhaust molecules by ambient air and effects on spacecraft charging. The project at the Naval Postgraduate School is under the cognizance of Distinguished Professor A. E. Fuhs who is principal investigator.

Reproduction of all or part of this report is authorized.

Prepared by:

Joseph Falcovitz

DR. JOSEPH FALCOVITZ
Research Contractor

Reviewed by:

Allen E Fuhs

ALLEN E. FUHS
Distinguished Professor & Chairman
Space Systems Academic Group

Released by:

G. E. Schacher

G. E. SCHACHER
Dean of Science and Engineering

REPORT DOCUMENTATION PAGE

1a. REPORT SECURITY CLASSIFICATION UNCLASSIFIED		1b. RESTRICTIVE MARKINGS NONE A183076													
2a. SECURITY CLASSIFICATION AUTHORITY		3. DISTRIBUTION/AVAILABILITY OF REPORT Approved for Public Release; Distribution Unlimited													
2b. DECLASSIFICATION/DOWNGRADING SCHEDULE															
4. PERFORMING ORGANIZATION REPORT NUMBER(S) NPS72-87-003CR		5. MONITORING ORGANIZATION REPORT NUMBER(S) NPS72-87-003CR													
6a. NAME OF PERFORMING ORGANIZATION JOSEPH FALCOVITZ	6b. OFFICE SYMBOL (If applicable) Code 72	7a. NAME OF MONITORING ORGANIZATION NAVAL POSTGRADUATE SCHOOL, CODE 72													
6c. ADDRESS (City, State, and ZIP Code) Research Contractor Naval Postgraduate School Monterey, CA 93943-5100		7b. ADDRESS (City, State, and ZIP Code) Space Systems Academic Group Monterey, CA 93943-5100													
8a. NAME OF FUNDING/SPONSORING ORGANIZATION Strategic Defense Initiative Office	8b. OFFICE SYMBOL (If applicable) SDIO/DEO	9. PROCUREMENT INSTRUMENT IDENTIFICATION NUMBER													
8c. ADDRESS (City, State, and ZIP Code) SDIO/DEO Washington, DC 20301-7100		10. SOURCE OF FUNDING NUMBERS <table border="1"><tr><td>PROGRAM ELEMENT NO.</td><td>PROJECT NO.</td><td>TASK NO.</td><td>WORK UNIT ACCESSION NO.</td></tr><tr><td></td><td></td><td></td><td></td></tr></table>		PROGRAM ELEMENT NO.	PROJECT NO.	TASK NO.	WORK UNIT ACCESSION NO.								
PROGRAM ELEMENT NO.	PROJECT NO.	TASK NO.	WORK UNIT ACCESSION NO.												
11. TITLE (Include Security Classification) AMBIENT SCATTERING FROM RING-SYMMETRIC SPACECRAFT EXHAUST PLUME															
12. PERSONAL AUTHOR(S) JOSEPH FALCOVITZ															
13a. TYPE OF REPORT Contractor Report	13b. TIME COVERED FROM JAN 87 TO MAR 87	14. DATE OF REPORT (Year, Month, Day) April 1987	15. PAGE COUNT 60												
16. SUPPLEMENTARY NOTATION															
17. COSATI CODES <table border="1"><tr><th>FIELD</th><th>GROUP</th><th>SUB-GROUP</th></tr><tr><td></td><td></td><td></td></tr><tr><td></td><td></td><td></td></tr><tr><td></td><td></td><td></td></tr></table>		FIELD	GROUP	SUB-GROUP										18. SUBJECT TERMS (Continue on reverse if necessary and identify by block number) Spacecraft Contamination, Exhaust Plume, Ambient Scattering, First Collision ←	
FIELD	GROUP	SUB-GROUP													
19. ABSTRACT (Continue on reverse if necessary and identify by block number) <p>We present a first-collision model for the evaluation of return flux from the exhaust plume of a ring-symmetric HF/DF laser in LEO, generated by an incident flux of ambient molecules traveling at orbital speed. The steady plume is bounded by a pair of lip-centered rarefaction fans, and unless spacecraft attitude enables incident air molecules to reach the plume through the cavitation regions that extend beyond these fans, the spacecraft is shielded from ambient scattering by its own plume. Assuming hard-spheres collisions, the first-collision model is given by a simple closed-form expression that can be regarded as a source term for scattered exhaust molecules. This source term is integrated numerically throughout the fan, yielding the flux arriving at some surface "target point". Quantitatively, it is shown that for a typical HF DF laser exhaust the contamination level generated by ambient scattering is not significant. It was found that the maximum return flux of HF-DF constitutes about 2% of the incident ambient flux; this ratio will be nearly constant for LEO altitudes. The value of this flux ratio is shown to be dependent on the molecular collision model; it may change upon replacing the hard-spheres approximation by a more realistic collision model. A possible modification of spacecraft charging by the exhaust was examined, including production of HF⁺ and DF⁺. The only significant effect seemed to be shadowing of the downstream half of the spacecraft at oblique orbital attitudes.</p>															
20. DISTRIBUTION/AVAILABILITY OF ABSTRACT <input checked="" type="checkbox"/> UNCLASSIFIED/UNLIMITED <input type="checkbox"/> SAME AS RPT <input type="checkbox"/> DTIC USERS		21. ABSTRACT SECURITY CLASSIFICATION UNCLASSIFIED													
22a. NAME OF RESPONSIBLE INDIVIDUAL ALLEN E. FUHS, Distinguished Professor		22b. TELEPHONE (Include Area Code) (408) 646-2948	22c. OFFICE SYMBOL Code 72												

ABSTRACT

We present a first-collision model for the evaluation of return flux from the exhaust plume of a ring-symmetric HF/DF laser in LEO, generated by an incident flux of ambient molecules traveling at orbital speed. The steady plume is bounded by a pair of lip-centered rarefaction fans, and unless spacecraft attitude enables incident air molecules to reach the plume through the cavitation regions that extend beyond these fans, the spacecraft is shielded from ambient scattering by its own plume. Assuming hard-spheres collisions, the first-collision model is given by a simple closed-form expression that can be regarded as a source term for scattered exhaust molecules. This source term is integrated numerically throughout the fan, yielding the flux arriving at some surface "target point". Quantitatively, it is shown that for a typical HF/DF laser exhaust the contamination level generated by ambient scattering is not significant. It was found that the maximum return flux of HF + DF constitutes about 2% of the incident ambient flux; this ratio will be nearly constant for LEO altitudes. The value of this flux ratio is shown to be dependent on the molecular collision model; it may change upon replacing the hard-spheres approximation by a more realistic collision model. A possible modification of spacecraft charging by the exhaust was examined, including production of HF^- and DF^- . The only significant effect seemed to be shadowing of the downstream half of the spacecraft at oblique orbital attitudes.

ACKNOWLEDGEMENTS

This work is part of a study involving gas dynamics of exhaust plumes from spacecrafts. It was conducted under the cognizance of Distinguished Professor Allen E. Fuhs, who initiated this research program at the Naval Postgraduate School. I wish to thank Professor Fuhs for his inspiring guidance and deeply appreciate his continued support.

Accession For	
NTIS CRA&I	<input checked="" type="checkbox"/>
DTIC TAB	<input type="checkbox"/>
Unannounced	<input type="checkbox"/>
Justification	
By	
Distribution /	
Availability Codes	
Dist	Avail and/or Special
A-1	



TABLE OF CONTENTS

1.	INTRODUCTION.....	1
2.	COMPUTATION OF THE PLUME FLOW FIELD.....	4
3.	AMBIENT SCATTERING.....	8
3.1	First Collision Model.....	8
3.2	Flux Integration Scheme.....	10
4.	RESULTS AND DISCUSSION.....	17
5.	SPACECRAFT CHARGING.....	23
6.	CONCLUDING REMARKS.....	27
7.	REFERENCES	29
	APPENDIX A. DESCRIPTION OF AMB CODE.....	31
A.1	Description of Subroutines.....	31
A.2	Listing of AMB code.....	34
8.	DISTRIBUTION LIST.....	52

LIST OF FIGURES

Figure 1-1.	Ring-Symmetric HF DF Laser Exhaust Plume	3
Figure 1-2.	Schematic Description of Ambient Scattering. The Cavitation Region is Bounded by Lines CA and CB	3
Figure 2-1.	Power $\delta(0,\beta)$ for the power-law Approximation.....	6
Figure 2-2.	Variation of Mach Number along Characteristic Line $\beta = 13$	7
Figure 3-1.	Incidence-Plane Description of Flux Integration Scheme	14
Figure 3-2.	Hard-Spheres Collision Notation	15
Figure 3-3.	Scattering Envelope for Hard-Spheres Collision.....	16
Figure 4-1.	Variation of Return Flux with Target Point (X_s). Target Point at Incidence-Plane ($\phi_A = 0$) and Constant Incidence-Angle ($\psi_A = 20^\circ$).....	20
Figure 4-2.	Variation of Return Flux with Ambient Incidence Angle (ψ_A). Fixed Target Point ($X_s = 1$ m) Located at Incidence-Plane ($\phi_A = 0$).....	21

Figure 4-3.	Variation of Return Flux with Ambient Azimuth Angle (ϕ_A). Fixed Target Point ($X_s = 1$ m) and Ambient Incidence Angle ($\psi_A = 20^\circ$).....	22
-------------	---	----

LIST OF TABLES

Table 4-1.	Typical Operating Conditions of HF/DF Laser Exhaust.....	19
------------	--	----

EMPTY PAGE

1. INTRODUCTION

This presentation is part of a study on the gas dynamics of ring-symmetric exhaust plumes in space, conducted at the Naval Postgraduate School in Monterey. A ring-symmetric jet has zero thrust, which makes it suitable as an exhaust configuration for various open loop power plants designed to produce high power for relatively short durations. One such system is an envisioned space-based chemical laser, shown schematically in Fig. 1-1. In the case of a chemical laser, a ring-symmetric configuration would also enable the laser radiation to emerge in the form of an axisymmetric beam.

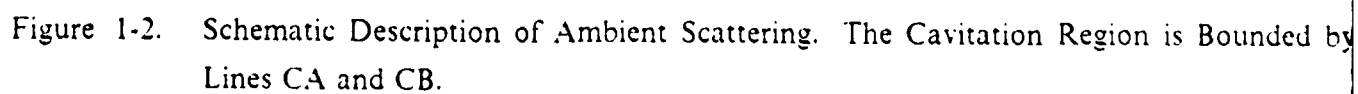
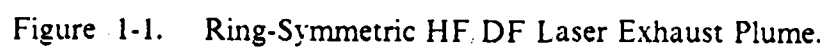
The exhaust nozzle should be designed to bring the outgoing flow to a supersonic speed at the nozzle exit surface. The near field of a free jet is then composed of an inner core bounded by a pair of ring-symmetric rarefaction fans centered at the nozzle lips (Fig. 1-1). Beyond the limiting characteristic surface of the centered rarefaction waves (CRW), a near-vacuum condition prevails. For the purpose of continuum gas dynamic analysis, we assume it is a perfect vacuum.

An earth orbiting vehicle is subject to an oncoming stream of ambient molecules at a speed of $U_A \approx 8$ (km/sec), in a direction depending upon its orientation relative to the orbital velocity vector. This speed is sufficiently high to cause backscattering of exhaust molecules (see schematic description in Fig. 1-2) moving at speeds appropriate to chemical combustion (about 2 to 4 km/s). However, large exhaust plumes, having achieved stationary flow, may be sufficiently dense at their outer fringes to effectively trap and entrain all oncoming ambient molecules. Thus, ambient scattering may be significant only in selected ranges of attitude angles, at which ambient molecules can reach the vicinity of the spacecraft by traveling almost collisionlessly through cavitation regions. Exhaust molecules that may be "candidates" for ambient scattering will hence come from plume segments flanked by cavitation regions. The contribution of ambient scattering to contamination will thus be highly dependent upon spacecraft geometry and orientation. This may well affect spacecraft design and operating procedures.

The purpose of this report is to present a first-collision model for estimating the flux of exhaust molecules backscattered from the fringes of the plume by ambient molecules, along with results of sample flux computations performed on a typical HF DF laser exhaust configuration. The flow field throughout the plume is assumed to be governed by the equations of continuum gas dynamics. In principle, the flow could be obtained by solving the governing equations, i.e., the equations for stationary isentropic flow in two-dimensional axisymmetric coordinates. In practice, this is normally

accomplished by integrating the flow equations in characteristic form, using some finite difference scheme (method-of-characteristics). We have performed such computations, but given the complexity of applying them to the subsequent integration of ambient scattering flux (due to the need for two-dimensional interpolations from an irregular solution grid), we opted for a different alternative: a closed-form approximation to the ring-symmetric CRW, based on an analytic expression for flow variables along characteristic lines that fan out from the nozzle lip.

The plan of this report is as follows. In Ch. 2 we outline the approximation to the ring-symmetric CRW and present some computation results that demonstrate its accuracy. In Ch. 3 we describe the first-collision model and the 3-D spatial integration scheme for computing the flux arriving at the cylindrical spacecraft. In Ch. 4 some results of backscattered flux of corrosive molecules ($\text{HF} + \text{DF}$), showing flux variation with target point location (X_s) and attitude angles (ψ_A, ϕ_A) are presented. In Ch. 5 we take up the subject of spacecraft charging, using results of ambient scattering to assess the effect of laser exhaust on spacecraft charging. This is followed by concluding remarks in Ch. 6 and a list of references in Ch. 7. A concise description of the flux computation code "AMB" is given in Appendix A, followed by the code listing.



2. COMPUTATION OF THE PLUME FLOW FIELD

Most ambient molecules entering the CRW that flanks the exhaust plume are stopped within several mean free paths from their point of entry. A quantitative estimate of ambient back-scattering would thus depend on the flow field at the outer (hypersonic) fringes of the lip-centered CRW. Even though the flow in those regions is generally past the surface of continuum breakdown, the density there is reasonably well approximated by the continuum flow field, as demonstrated by Bird's Monte-Carlo simulation of a Prandtl-Meyer expansion to vacuum [1]. The evaluation of ambient scattering thus calls for an ancillary computational procedure capable of rendering the continuum flow field at a large number of points in the ring-symmetric CRW of an exhaust plume. This method was described in a recent report [2]. Here we just outline the key ideas and main results of this approximation method.

Our analytic approximation to a ring-symmetric CRW is formulated as follows. In a planar CRW (Prandtl-Meyer flow) all flow variables are uniform along the characteristic lines that fan out from the corner (we assume they are the C^+ family). In the ring-symmetric case the flow near the corner approaches asymptotically a corresponding planar CRW flow, which we term the *associate* CRW. However, the gradients along C^+ characteristics at the corner of a ring-symmetric CRW do not vanish as in a planar CRW. The key idea is thus: evaluate flow gradients in C^+ directions at the corner, then use them to extrapolate the associate CRW along C^+ lines to a finite distance from the corner. The extrapolation is a nonlinear function of the radial coordinate y , chosen so that the ensuing expression conforms exactly to the flow at the leading (exit) characteristic $C^+(\beta_1)$. Omitting all details of the analysis, the resulting approximation is presented as the following power-law:

$$f(\alpha, \beta) = f(0, \beta) [y(\alpha, \beta)/y(0, \beta)]^{\delta(0, \beta)} \quad (2-1)$$

where f is the streamtube area ratio for isentropic flows ($f=1$ at a sonic point), β is the Mach number of a particular characteristic line at the corner, α is a coordinate along the $C^+(\beta)$ characteristic line ($\alpha=0$ at the corner), and y is the radial coordinate of a point on the characteristic line $C^+(\beta)$. The Mach number at point (α, β) is readily determined from $f(\alpha, \beta)$ using the standard relation between area ratio and Mach number [3]. A closed-form expression for $\delta(0, \beta)$ was developed but is not given here; instead, this function is shown in Fig. 2-1. We note that δ approaches the asymptotic value of $2/(3-\gamma)$ as β increases to infinity, and that generally $1 < \delta(0, \beta) < 2$ so that streamtubes diverge at a rate intermediate between that of cylindrical and spherical expansion flows.

Clearly, in an isentropic flow all thermodynamic variables, and in particular density, can be evaluated from f . This approximation is readily applied to the hypersonic portions of a ring-symmetric CRW since it turns out that characteristic lines are nearly straight there, which means that the characteristic line $C^+(\beta)$ passing through a given point can be readily determined. As a demonstration of the degree of accuracy obtainable from this approximation, we show in Fig. 2-2 the variation of Mach number along a characteristic line in the ring-symmetric CRW, compared with an accurate method-of-characteristics computation. This comparison demonstrates that the analytic approximation is reasonably accurate to nearly ten corner-radii away from the corner.

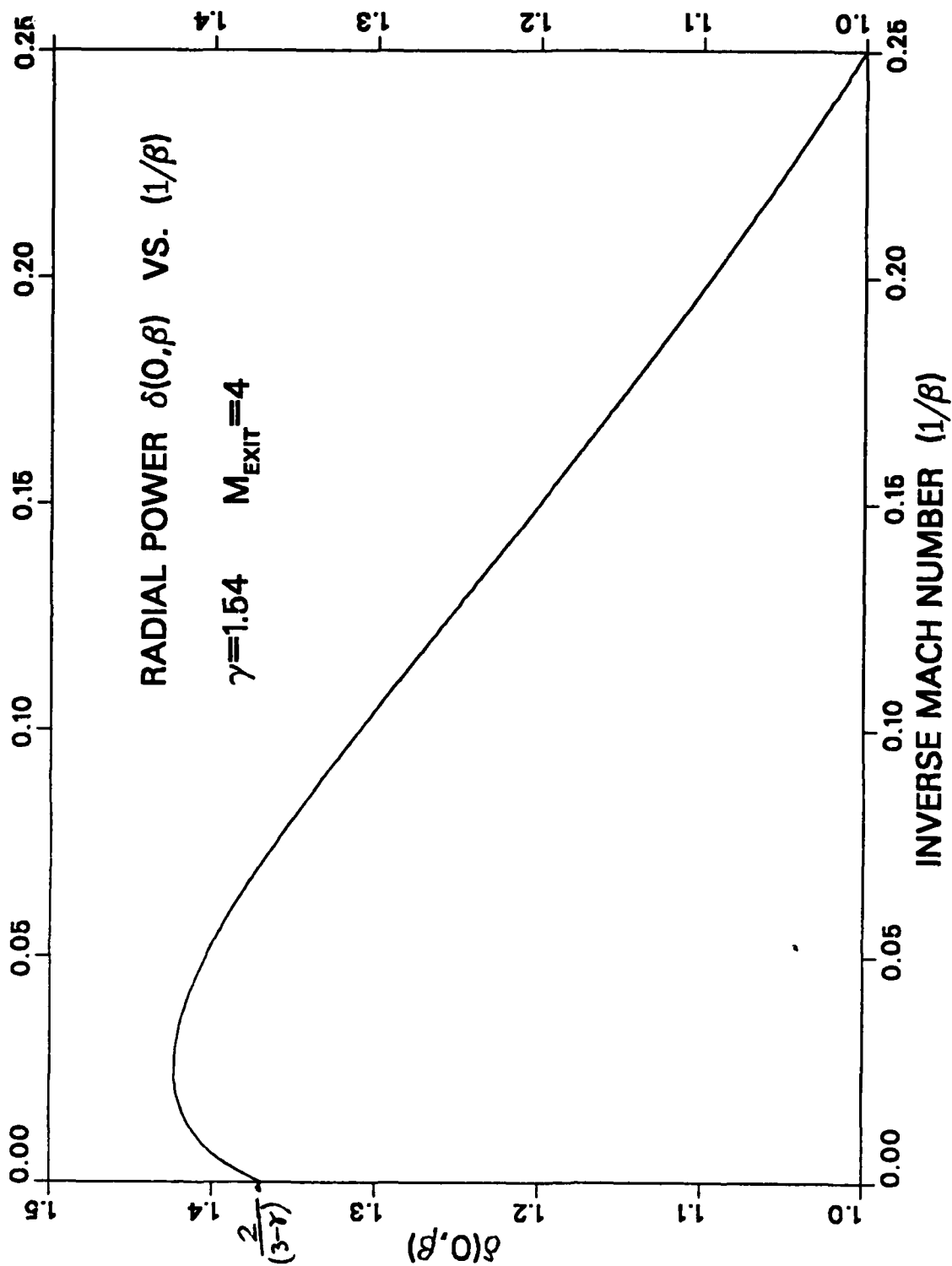


Figure 2-1. Power $\delta(0,\beta)$ for the power-law Approximation.

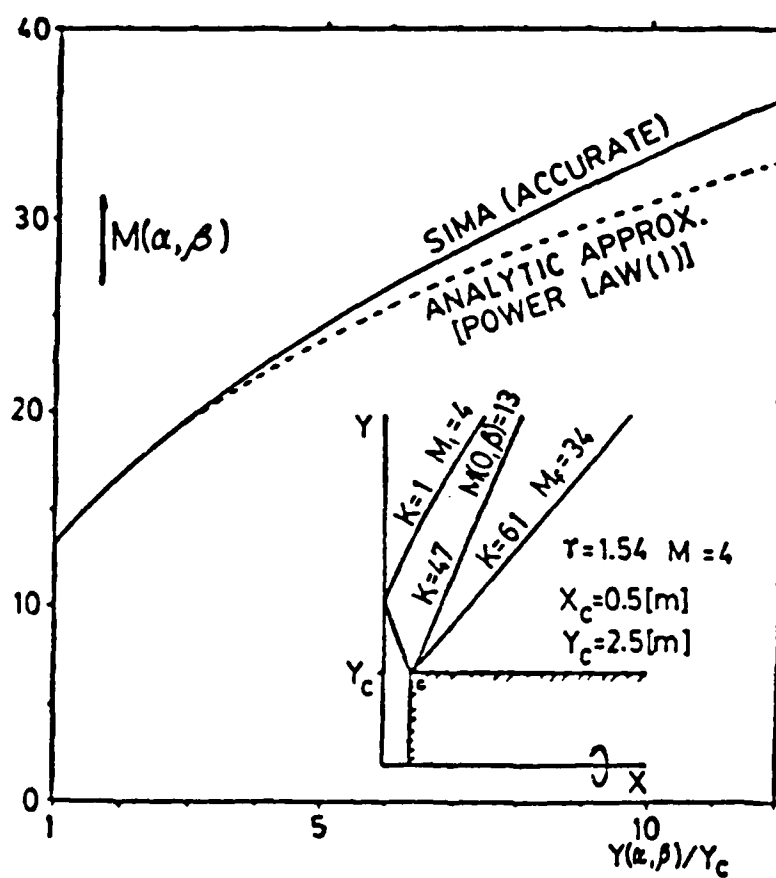


Figure 2-2. Variation of Mach Number along Characteristic Line $\beta = 13$.

3. AMBIENT SCATTERING

When a rocket or laser exhaust is released into space from an earth-orbiting spacecraft, it encounters an oncoming stream of ambient molecules flowing at the orbital speed of $U_A \approx 8$ (km/sec). At altitudes higher than 200 (km), the air mean free path exceeds 250 (m), so that it is considerably larger than almost any spacecraft. Consequently, ambient molecules would hardly be subjected to a shock transition prior to their impact at the spacecraft or exhaust plume. In this chapter we describe the formulation of the first-collision model in Section 3.1 and then proceed to present the derivation of the flux integration scheme for hard-sphere collisions in Section 3.2.

3.1 First Collision Model

The highest ambient number density that we consider for earth-orbiting spacecrafts is $N_A = 1 \times 10^{16}$ (m^{-3}), which roughly corresponds to Sunspot Maximum at 200 (km) [4]. The typical laser exhaust (Table 4-1) would reach a number density of about 2×10^{19} (m^{-3}) at the very high Mach number of 30. Hence, ambient flux constitutes just a slight perturbation to the near-field portion of a typical laser exhaust plume. Obviously, ambient molecules that penetrate the plume, would subsequently be entrained by the main flow. But how far do they penetrate? And would exhaust molecules scattered by them reach the spacecraft? In seeking answers to these questions, we are led to some interesting observations concerning ambient scattering.

Consider the HF laser depicted in Fig. 1-1. The spacecraft diameter is 5 (m) and the centrally located ring-symmetric nozzle is 1 (m) wide. Typical operating conditions (Table 4-1) are assumed. They are based on some experimental HF DF laser studies conducted at TRW [5,6]. Suppose that the spacecraft axis is normal to the orbital velocity vector (normal incidence). Let the plane of incidence be the plane defined by the intersection of the spacecraft axis with the orbital velocity vector. The probability that an ambient molecule traveling in the plane of incidence would reach the spacecraft collisionlessly is $\exp(-\eta)$, where η is its expected number of collisions with exhaust molecules. We define the number η as "molecular thickness", in analogy to "optical thickness". So in order to determine the extent to which ambient molecules at normal incidence reach the spacecraft, we seek the distribution of radial molecular thickness as function of distance from the spacecraft mid-plane (normal to axis at its midpoint).

For this purpose we computed the ring-symmetric exhaust flow field, using a semi-inverse marching characteristics scheme [7]. The marching was in the radial direction, starting with uniform flow at the nozzle exit; the computation was carried on until it became evident that even at a distance of 20 (m) from the mid-plane, the radial molecular thickness was well over 40. The entire spacecraft was thus shielded from any ambient scattering at (or near) normal incidence. This shielding effect has two significant implications which we discuss briefly below.

- (a) It is present only during stationary exhaust flow. At startup and shutdown phases, ambient scattering may be substantial even at normal incidence.
- (b) During the stationary phase, ambient scattering is substantial only at attitude angles that enable ambient molecules to reach the vicinity of the plume by traveling through "molecularly thin" cavitation regions that flank the plume. We thus anticipate a decisive dependence of ambient scattering on attitude variations, whenever those variations steer the spacecraft into or out of a shielded posture.

As a first attempt at a quantitative estimate of ambient scattering flux, we have formulated a simple first-collision model of this effect. In the sequel we present an outline of the model, along with some sample results evaluated for an HF laser configuration identical to that considered for the shielding effect mentioned above.

The basic idea is the following. Ambient molecules entering an exhaust plume, require several collisions to become fully "accommodated" with the main flow (i.e., to be entrained by the main flow at the prevailing flow velocity and temperature). One may reasonably approximate this process by considering just one collision - the first.

With the help of some additional assumptions, we were able to derive a closed form expression for the flux of exhaust molecules that arrive at the spacecraft following a first collision with an ambient molecule. The main assumptions of this model are :

- (1) **FIRST COLLISIONS:** Only first collisions for either ambient or exhaust molecules are considered. Hard-spheres elastic collisions are assumed. Upon a second collision of either an ambient or an exhaust molecule, it is considered "lost" (i.e., it joins the main flow). Collisions of ambient molecules with spacecraft surfaces are ignored. Ambient molecules are assumed to traverse cavitation regions collisionlessly.

- (2) **COLD FLOW:** The oncoming ambient air flow is deemed "cold"; i.e., all molecules move at the uniform orbital velocity. The same "cold" assumption is applied to the exhaust flow, since most ambient scattering takes place at plume regions of very high Mach numbers (well over 10, in the present case).
- (3) **CRW Flow Field:** ring-symmetric CRW flow field is determined from the power-law approximation described in Ch. 2 above. This approximation approaches Prandtl-Meyer flow at points whose distance from the nozzle lip is much smaller than the spacecraft radius.

Based on these assumptions, ambient scattering is represented as a source term for side-scattered exhaust molecules, distributed throughout the lip-centered rarefaction fan. The total flux arriving at a specified point on the cylindrical spacecraft is readily computed by integrating numerically that source distribution over the entire ring-fan.

The highlights of the spatial integration scheme (Fig. 3-1) are as follows. The limiting characteristic surface ($M = \infty$) of the ring-symmetric CRW is divided into surface elements formed by dividing the surface into a set of ring-strips which are subdivided in the circumferential (azimuthal) direction (φ) into surface elements. The line-of-sight ($\vec{\Omega}$) from the "target point" on the spacecraft to the center of each surface element is extended into the ring-symmetric CRW, and flux integration using the first-collision source term with appropriate weight factors is performed along this line until convergence is attained. Contributions from each surface element are summed, taking care to disregard portions of the ring-symmetric CRW that are shadowed by the cylindrical spacecraft (either the line-of-sight or the trajectory of oncoming ambient molecules may be shadowed). Some further details of the flux integration scheme and hard-spheres collisions are provided in Section 3.2 below.

3.2 Flux Integration Scheme

The description of the first collision model is hereby supplemented with an outline of the expressions used in the flux integration and their derivation. The integration scheme for flux arriving at point X_s on the spacecraft is depicted in Fig. 3-1. Note that only the plane of incidence is shown in Fig. 3-1; at other azimuth angles the geometry is not co-planar, so 3-D geometrical expressions are used to get the coordinates (ψ, φ and radial distance $(y^2 + z^2)^{1/2}$) from $\vec{\Omega}$ and S ; the derivation of these geometrical relations is straightforward, so that we omit these details in the present report. The total number flux $Q_i(X_s)$ of i exhaust molecules arriving at point X_s is given by the following expression :

$$Q_i(X_s) = \int d^3\vec{\Omega} \cos\alpha_s \sum_k \int_0^\infty dS \sigma_{ik} h_i N(S) h_k N_A |\vec{U}(S) - \vec{U}_A| \exp[-\eta_k(S)] P_{ik}(S, -\vec{\Omega}) \exp[-\eta_{ik}(S)]$$

$$\eta_k(S) = \sum_j \int_0^{t(S)} dt' \sigma_{ik} h_i N(t') |\vec{U}(t') - \vec{U}_A| / |\vec{U}_A| \quad (3-1)$$

$$\eta_{ik}(S) = \sum_j \int_0^S dS' \sigma_{ij} h_j N(S') |\vec{U}_{ik}(S') - \vec{U}(S')| / |\vec{U}_{ik}(S')|$$

$()_i$ $()_j$ - Exhaust species

$()_k$ - Ambient species

These expressions are interpreted as follows. The collision depicted in Fig. 3-1 is between exhaust molecule m_i and ambient molecule m_k . The exhaust molar fractions h_i and ambient molar fractions h_k are assumed uniformly constant, and so are the ambient velocity \vec{U}_A and number density N_A . The exhaust velocity $\vec{U}(S)$ and number density $N(S)$ are function of the location in the flow field defined by $\vec{\Omega}$ and S . These flow variables are computed by first evaluating the coordinates of point $\vec{\Omega}.S$ (Fig. 3-1) in the ring-symmetric CRW from the 3-D geometry, and then employing the power-law approximation outlined in Ch. 2 above, to get all flow variables for a ring-symmetric CRW. In this computation we exploit the fact that characteristic lines fanning out from the nozzle lip are nearly straight lines at the low pressure side of the ring-symmetric CRW.

The $\vec{\Omega}$ integration is performed numerically according to the scheme outlined in Section 3.1 above, as a summation over elements of solid angle ($\Delta^3\vec{\Omega}$) subtended by area elements on the limiting characteristic cone ($\psi = \psi_f$).

The S integration is considerably more complex. The integrand for this integration is derived as follows. Denote by L the line-of-sight distance between point X_s and fan point $\vec{\Omega}.S$. A volume element at the fan point is given by $\Delta v = L^2 \Delta S \Delta^3\vec{\Omega}$. The number of ik pair collisions in Δv per unit time is $\sigma_{ik} h_i N(S) h_k N_A |\vec{U}(S) - \vec{U}_A| \exp[-\eta_k(S)] \Delta v$, where $\eta_k(S)$ denotes the expected number of collisions of ambient molecule k with any exhaust molecule, between its point of entry into the plume and point $\vec{\Omega}.S$. We now multiply this term by $\exp[-\eta_{ik}(S)]$ which is the probability that exhaust molecule i scattered by ambient molecule k would travel from point $\vec{\Omega}.S$ to point X_s collisionlessly, where $\eta_{ik}(S)$ is the expected number of collisions for this path segment. (Note that in Eq. (3-1) the summation in the expression for $\eta_{ik}(S)$ is over all exhaust species j).

The final step in constructing the integrand for the S integration involves the post-collision directional distribution function $P_{ik}(S, -\vec{\Omega})$, whose derivation will be given in the sequel. We multiply the integrand by $P_{ik}(S, -\vec{\Omega}) \Delta^3 \vec{\Omega}_c$ which is the fraction of i exhaust molecules scattered by k ambient molecules into a solid angle element $\Delta^3 \vec{\Omega}_c$ about the unit vector $-\vec{\Omega}$. Considering the flux arriving at a surface area element ΔA_s around point X_s , the solid angle element subtended by ΔA_s is $\Delta^3 \vec{\Omega}_c = \Delta A_s \cos \alpha_s / L^2$. Eq. (3-1) for $Q_i(X_s)$ now follows upon dividing the resulting expression by ΔA_s , thus referring the arriving flux to a unit area at the point of arrival X_s .

Numerically, the S integration was performed using the classical Runge-Kutta scheme (fourth order). The integration for $\eta_{ik}(S)$ and $\eta_k(S)$ has to be repeated at each point S . We found reasonable convergence with 4 points in the $\eta_k(S)$ integration and 6 points in the azimuth integration. The S integration was terminated when convergence was attained (this is the meaning of the upper limit ∞ in the S integral in Eq. (3-1)). The summation over new strips on the limiting cone ($\psi = \psi_f$) was also terminated upon convergence. The CPU time consumed per target point was about 100 (sec) on IBM 3033 mainframe.

We now take up the derivation of an expression for the post-collision directional distribution function $P_{ik}(S, -\vec{\Omega})$, which we denote hereafter as $P(-\vec{\Omega})$. We adopt the pair-collision notation presented in Fig. 3-2 for the hard-sphere collision analysis.

As a consequence of conservation of momentum and energy (elastic collisions), the center-of-mass velocity \vec{C}_m and the magnitude of the relative velocity \vec{C}_r are unchanged by the collision [8]. The post-collision velocities are given by :

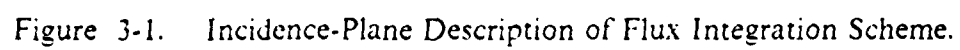
$$\begin{aligned}
 \vec{C}_1^* &= \vec{C}_m + \mu_2 \vec{C}_r^* & \vec{C}_2^* &= \vec{C}_m - \mu_1 \vec{C}_r^* \\
 \vec{C}_r &= \vec{C}_1 - \vec{C}_2 & \vec{C}_r^* &= \vec{C}_1^* - \vec{C}_2^* \\
 \mu_1 &= m_1 / (m_1 + m_2) & \mu_2 &= m_2 / (m_1 + m_2) \\
 \vec{C}_m &= \mu_1 \vec{C}_1 + \mu_2 \vec{C}_2 & |\vec{C}_r^*| &= |\vec{C}_r|
 \end{aligned}
 \tag{3-2}$$

The only free parameter in the expressions for post-collision velocities is the orientation of the post-collision relative velocity \vec{C}_r . This orientation is uniformly likely to be in any direction in space when hard-spheres collision is assumed [8], as represented by the spherical scattering envelope in

Fig. 3-3. The probability of obtaining \vec{C}_1^* in solid angle element $\Delta^3\vec{\Omega}$ about $-\vec{\Omega}$ (Fig. 3-3) is given by :

$$P(-\vec{\Omega}) = (1/4\pi |\mu_2 \vec{C}_r|^2) (\Delta A / \Delta^3\vec{\Omega}) = (1/4\pi |\cos\delta|) (|\vec{C}_1^*|^2 / |\mu_2 \vec{C}_r|^2) \quad (3-3)$$

where ΔA is an area element on the scattering envelope, whose projection on a plane normal to $\vec{\Omega}$ is $\Delta A |\cos\delta|$. We note that the origin of \vec{C}_m in Fig. 3-3 is external to the scattering envelope, resulting in two possible scattering elements on the sphere. In all the cases that we computed, however (see Ch. 4 below), that point was found to be always internal, so that there was only a single scattering solution with post-collision velocity $\vec{U}_{ik}(S)$ pointing at the spacecraft for any ik pair collision.



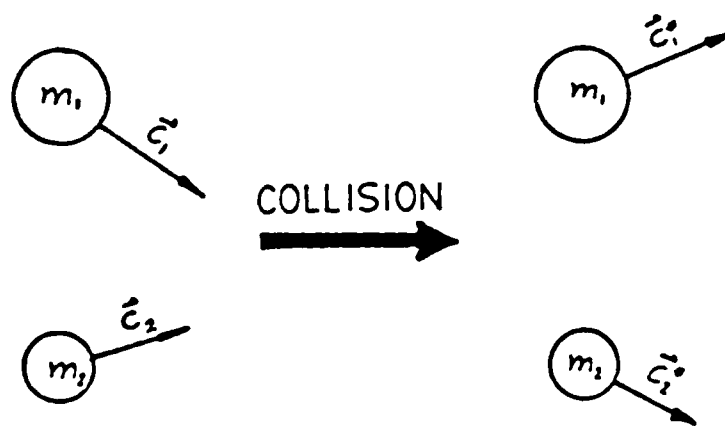


Figure 3-2. Hard-Spheres Collision Notation.

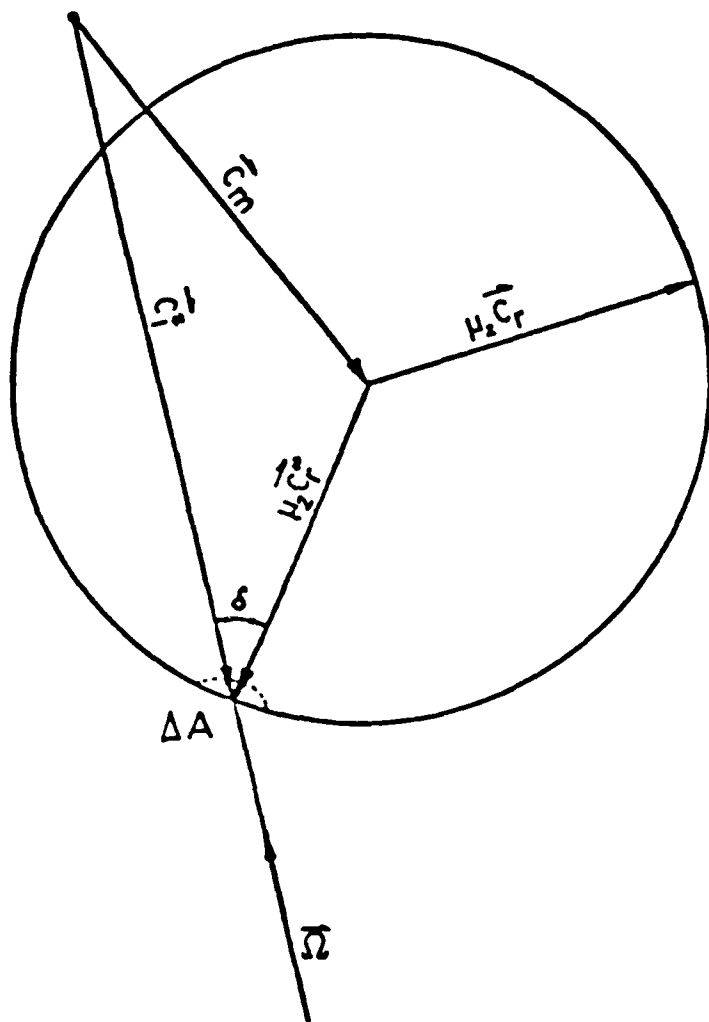


Figure 3-3. Scattering Envelope for Hard-Spheres Collision.

4. RESULTS AND DISCUSSION

We performed several computations of return flux generated by ambient scattering, aimed at demonstrating the expected flux level and its variation with spacecraft target point and orbital attitude angles. In all these computations we assumed that the exhaust flow is as in the typical HF/DF laser case (Table 4-1 below), and that the ambient density and velocity are $N_A = 1 \times 10^{16}$ (molecules/m³) and $U_A = 8$ (km/sec). As an approximation we further assumed that the sole ambient species is molecular nitrogen (molecular weight $W_A = 28$) and that all binary collision cross-sections are uniformly given by $\sigma = \pi D^2$, where D is the molecular diameter (Table 4-1). In each computation we evaluated the combined HF + DF flux by assuming that the molar fraction of DF is zero and the molar fraction of HF is the combined value for both species (Table 4-1) : $.091 + .135 = .226$. This is justified by the relatively small difference in molecular weight (just 5%) between these two species.

Three sets of flux computation were performed as follows :

- (a) Incidence-plane ($\phi_A = 0$) target points at various distances from the nozzle lip ($X_s = .1$ to $X_s = 10$ (m)), and at constant incidence angle ($\psi_A = 20^\circ$). The results are shown in Fig. 4-1. We observe that the flux is fairly insensitive to X_s . Also shown in Fig. 4-1 are flux computations where the ring-symmetric CRW flow is approximated as a planar CRW (Prandtl-Meyer flow), rather than the power-law as in Eq. (2-1) above. The planar case exhibits a somewhat higher flux, particularly at large X_s .
- (b) Incidence-plane ($\phi_A = 0$) target points at $X_s = 1$ (m) and at various incidence angles ($\psi_A = 0$ to $\psi_A = 40^\circ$). A polar representation of the results is given in Fig. 4-2. Note the sharp decrease in flux as the incidence angle ψ_A approaches the plume limiting angle $\psi_r = 41^\circ$.
- (c) Azimuth angle variation ($\phi_A = 0$ to $\phi_A = 180^\circ$) at a constant location ($X_s = 1$ (m)) and at a constant angle of incidence ($\psi_A = 20^\circ$). A polar representation of the results is given in Fig. 4-3. Observe that flux becomes sensitive to azimuth angle ϕ_A only past $\phi_A = 90^\circ$, where shadowing by the cylindrical spacecraft becomes increasingly dominant.

In addition to return flux we also computed the rms velocity of the arriving molecules. For the target points in group (a), the rms velocity varied between 6000 and 6600 (m/sec) (the higher velocity at smaller X_s), which corresponds to a kinetic energy of about 4 (ev) per molecule (HF).

The maximum return flux arriving at the spacecraft is about 0.15×10^{19} (molecules/m²sec), which corresponds to a surface deposition rate of about 300 monolayers (HF + DF) per hour. This level of contaminating flux may seem to be not outright negligible; however, since return flux is proportional to ambient density, it will be scaled down considerably at higher altitudes (and lower ambient densities).

We observe that the maximum return flux constitutes a fraction of about 2% of the incident ambient flux. This return flux ratio is roughly maintained at almost all target points and attitude angles in groups (a), (b) and (c). The only exceptions are incidence angles near the limiting cone ($\psi = \psi_r$) or at azimuth angles $\phi_A > 125^\circ$ where shadowing becomes dominant. This observation is interpreted as follows.

Consider the total solid angle subtended by the limiting cone (considered to be infinitely extended in the axial direction) as viewed from a target point (for all lines-of-sight $\vec{\Omega}$ pointing outward of the cylindrical spacecraft surface). It is independent of target location due to the "self-similar" geometry. During each flux computation, we also evaluated the total solid angle subtended by that segment of the cone over which the flux integration was actually performed (see Section 3.2). It was found out that for all but the "shadowed" cases ($\phi_A > 125^\circ$), this solid angle constituted a fraction of $86 \pm 1\%$ of the solid angle subtended by the infinite cone. We interpret this result as a hint that geometrical "view factors" arising in the course of the flux integration, are not the dominant factor in determining the 2% level of flux ratio. What then are the dominant factors?

For a possible explanation we turn to the flux integration scheme presented in Section 3.2. The flux ratio is obtained upon dividing the integrand in Eq. (3-1) by $N_A U_A$ and setting $h_k = 1$ (since we assume a single species air). The major factors in the flux ratio integrand appear to be the no-collision probabilities $\exp[-\eta_{ik}(S)]$ and $\exp[-\eta_k(S)]$, and the post-collision directional distribution function $P_{ik}(S, -\vec{\Omega})$. The flux-averaged values of these functions in the group (a) computations were found to be as follows: $P_{ik}(S, -\vec{\Omega}) = .09$ to $.10$, $\eta_{ik}(S) = .42$ to $.54$ and $\eta_k(S) = .35$ to $.47$. The flux-averaged Mach number for group (a) points exhibited a much larger variation: between 30 and 80, with the higher Mach numbers obtained at further target points.

These results are interpreted as follows. The ambient no-collision probability $\exp[-\eta_k(S)]$ is sufficiently close to unity, so that in an order-of-magnitude analysis such as the present one, we may disregard this factor. If the velocity ratio in the $\eta_{ik}(S)$ integral of Eq. (3-1) is assumed to be unity (its average value for group (a) points is about 1.4), then the differential in the flux S integration becomes

$\sigma N(S) dS = d\eta_{ik}(S)$. This implies that the flux S integration results in some average value of the only remaining factor: $h_i P_{ik}(S, -\vec{\Omega})$. Since the $\vec{\Omega}$ integration introduces a factor of order unity, the order-of-magnitude estimate for the arriving-to-incident flux ratio is $[h_i P_{ik}(S, -\vec{\Omega})]_{av}$. The value of this estimate is $[h_i P_{ik}(S, -\vec{\Omega})]_{av} = .226 \times .09 \approx .02$, which is about equal to the actual flux ratio for target points in group (a).

When an exhaust flow and orbital parameters (velocity and attitude) are specified, $P_{ik}(S, -\vec{\Omega})$ depends on the choice of molecular collision model (we chose hard spheres), while h_i is uniformly constant. The foregoing reasoning thus establishes the collision model as a significant factor in determining ambient scattering flux levels, to the extent that $P_{ik}(S, -\vec{\Omega})$ is sensitive to the choice of model.

Table 4-1. Typical Operating Conditions of HF/DF Laser Exhaust

Mole fractions	[H] = .091 [HF] = .091 [H ₂] = .104 [DF] = .135 [He] = .579
Average molecular weight	7.14
Specific heats ratio	1.54
Stagnation temperature and density	1400 (K) .0075 (kg. m ³)
Exit Mach number	4.0
Molecular diameter (hard spheres)	2.5×10^{-10} (m)
Spacecraft diameter	5.0 (m)
Nozzle aperture	1.0 (m)

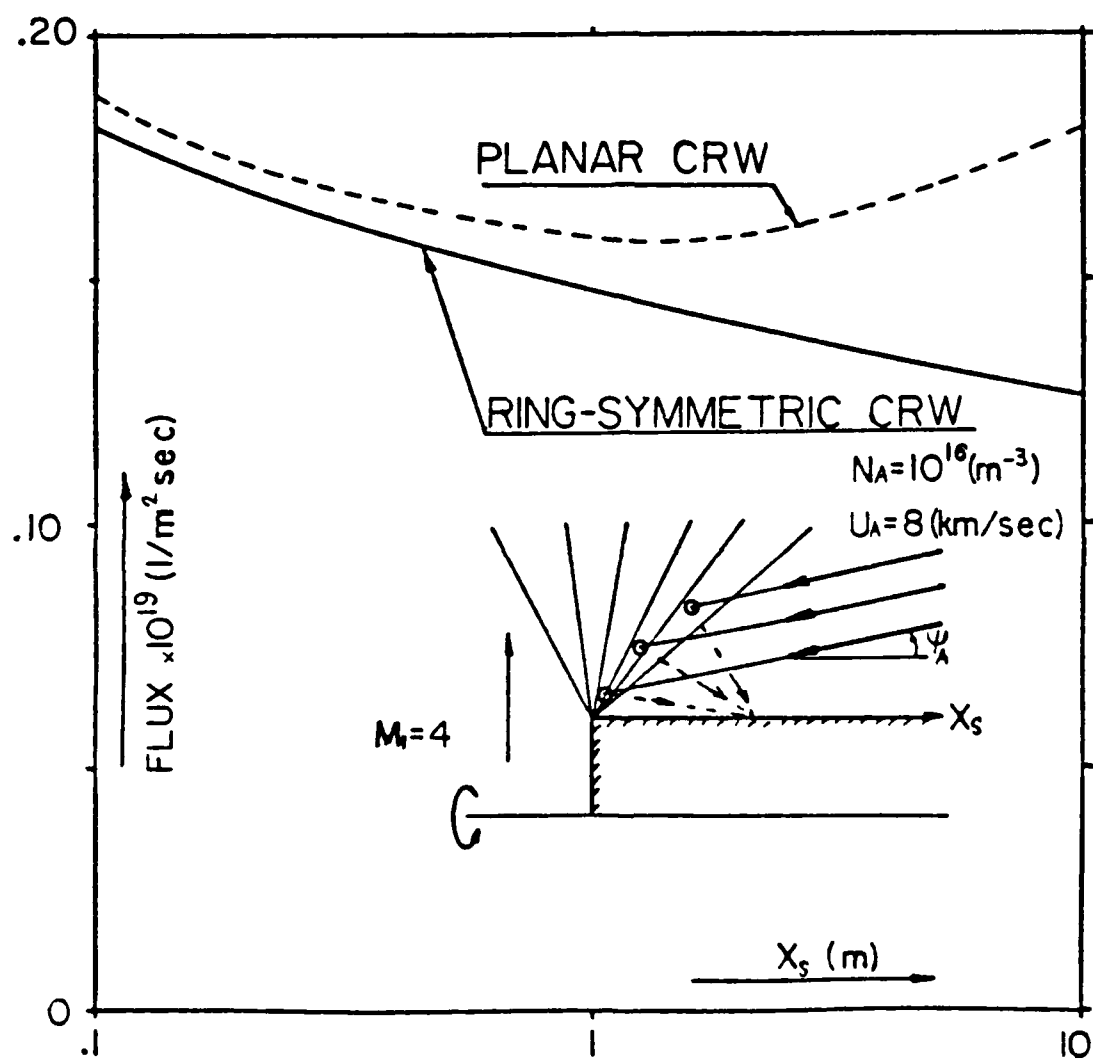


Figure 4-1. Variation of Return Flux with Target Point (X_s). Target Point at Incidence-Plane ($\phi_A = 0$) and Constant Incidence-Angle ($\psi_A = 20^\circ$).

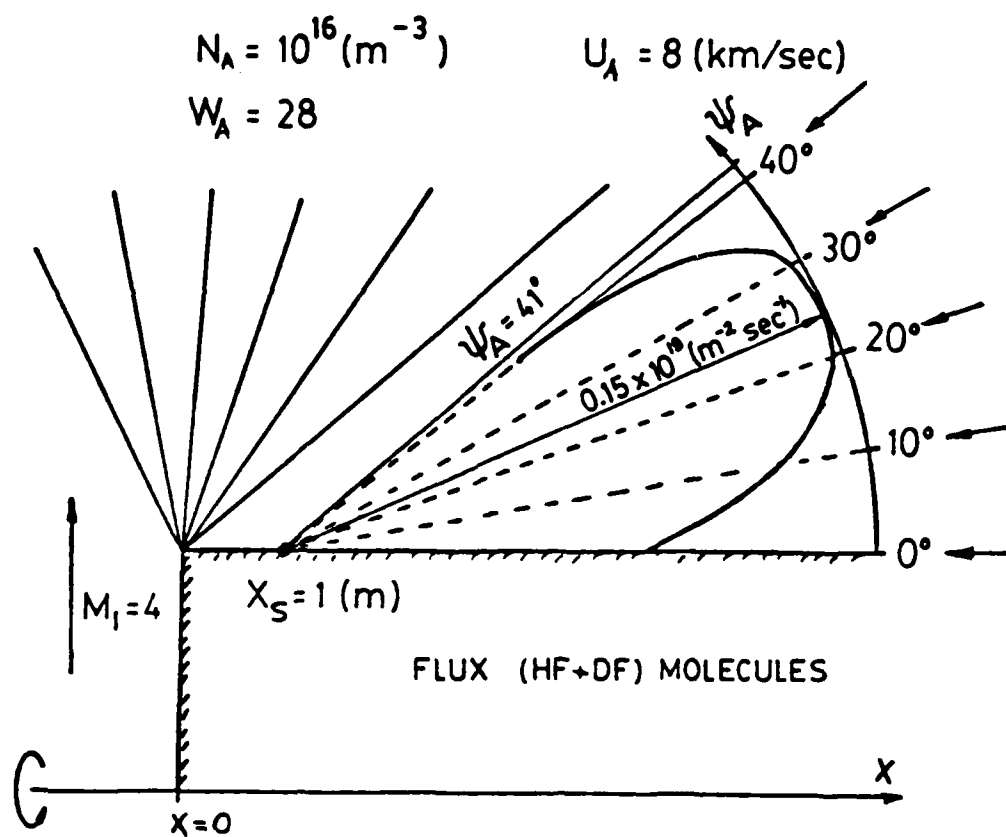


Figure 4-2. Variation of Return Flux with Ambient Incidence Angle (ψ_A). Fixed Target Point ($X_s = 1 \text{ m}$) Located at Incidence-Plane ($\phi_A = 0$).

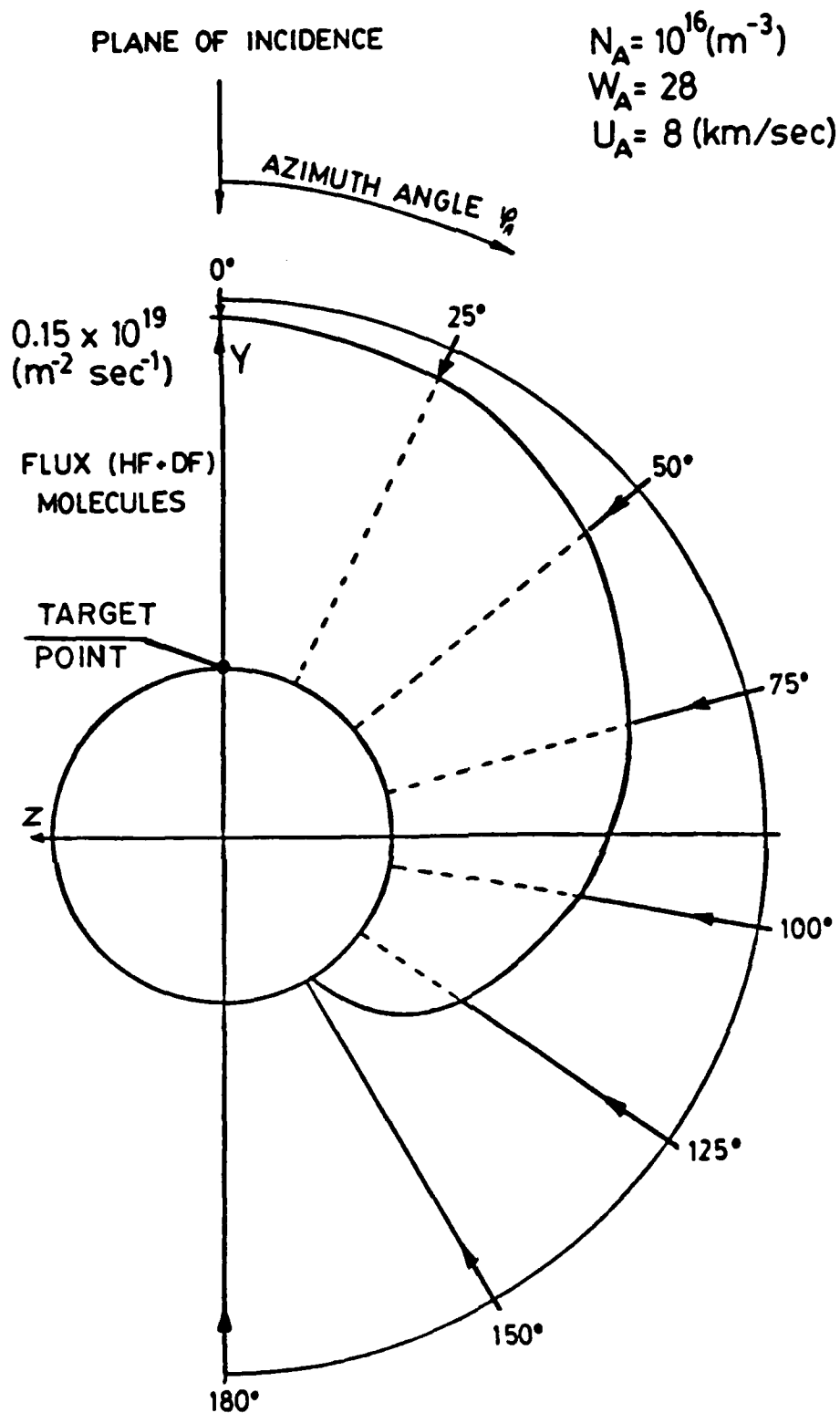


Figure 4-3. Variation of Return Flux with Ambient Azimuth Angle (ϕ_A). Fixed Target Point ($X_s = 1 \text{ m}$) and Ambient Incidence Angle ($\psi_A = 20^\circ$).

5. SPACECRAFT CHARGING

Spacecraft charging is a major concern to spacecraft designers, particularly for missions in GEO and to a lesser extent also in LEO. The exhaust plume of an HF/DF laser operating in the ionosphere (300 to 1000 km altitude) may modify significantly the pre-firing charging pattern of the spacecraft. Two classes of effects may lead to charging modification; they are:

- (a) The exhaust contains large concentrations of HF and DF molecules which are highly electronegative. They may be readily ionized by environmental electrons and change the existing spacecraft charging pattern.
- (b) When the spacecraft is oriented obliquely relative to its orbital velocity and the ambient plasma impinges at the plume boundary, the plume will cast a "shadow" on the downstream side, leading to a very dissimilar charging fluxes on the upstream and downstream halves of the spacecraft.

The knowledge gained in analyzing the ambient scattering effect can be applied to the assessment of the effects of ionospheric plasma on spacecraft charging. We first consider the upstream side of the spacecraft as mentioned in (a) above.

We contend that the exhaust-plasma interaction will not drastically alter the charging pattern of the upstream half. This assessment is established as follows. Consider the fact that ionospheric plasma has a particle number density no higher than $10^{12} \text{ (m}^{-3}\text{)}$ and energy per particle of at most 1 (ev) (excluding the auroral plasma of polar zones or events of sun storms, where the energy per particle is much higher). Significantly, the Debye length at the highest plasma density is very small: only about 10^{-3} (m) ; the largest Debye length in the ionosphere is 10^{-1} (m) [9]. Ion thermal velocity is typically lower than orbital velocity, but electron velocity is considerably higher than orbital velocity (at 1 ev the electron velocity is about $U_e = 6 \times 10^5 \text{ m/sec}$). Hence, ions would typically impinge at the plume as a uniform ion beam with the orbital velocity (like ambient molecules), while electrons are expected to impinge at the plume with their random-oriented thermal velocity.

In view of the results of ambient scattering analysis (Ch. 3 and 4 above), and since ions are subject to similar collision process with exhaust molecules as neutrals, ions will be stopped at the plume fringes much like ambient molecules. By virtue of the small Debye length (typically much smaller than the stopping distance), electrons would not penetrate any further than ions, regardless of their

collision cross-section with exhaust molecules. The familiar plasma sheath that forms at a solid surface, is hence replaced at the plume/plasma boundary by a typically neutral layer whose thickness is of the order of an ion/neutral mean free path, but much larger than the Debye length. Only at the upper altitude range of the ionosphere does the Debye length become comparable to a plume boundary mean free path (about .1 m), but there plasma density and flux are several orders of magnitude lower and charging modification is not likely to be significant at the relatively short firing duration of about 5 minutes.

Elastically scattered ions can be deflected towards the spacecraft as a result of elastic collisions with exhaust molecules, much like neutrals. Referring to our analysis of the return-to-ambient flux ratio (Ch. 4 above), it is clear that the relevant ratio here will be about $1/4\pi$, i.e., of the order of 10% (this is due primarily to the role played by the elastic directional distribution function — see Ch. 4). A change in the plasma-to-surface current of that order is hence possible, but unlikely to affect spacecraft design or operation significantly. The reason is that a design capable of smoothing away the inhomogeneous charge flux at oblique attitudes, will not be sensitive to a change in flux pattern of the order of 10% (in other words, potential differences may be amplified by 10%, which is hardly likely in a sound design to bring about arcing or other threshold phenomena).

Another effect which may potentially be significant in the upstream half is generation of electronegative species (HF^- , DF^-) by plasma electrons impinging at the plume. In the sequel, we examine the magnitude of this effect, concluding that it is negligible.

This estimate is best done by considering \dot{N}^- , which is the rate of production of HF^- and DF^- per unit volume, at a typical point in the exhaust where local Mach number is $M=30$ (this is typically the lowest average Mach number for the plume region where ambient scattering takes place — see Ch. 4 above). Since energy is released by the electronegative ion formation, the reaction involves a third body as follows :



where M is the third body molecule. We assume a simplified classical kinetic model for this reaction, as follows. The pair $\text{HF} M$ collide with a frequency proportional to the local number density and HF molar fraction, and to the average relative velocity. An electronegative ion formation can occur only if an electron collides with the pair during their collision, which lasts $t_c = D/\bar{C}_r$, where \bar{C}_r is the average relative pair velocity. Based on this classical model, and assuming the same cross-section for

electronegative ion formation as for elastic HF/M collisions, the volume rate of electronegative ion generation is given by :

$$\dot{N}^- = (\pi D^3 N) N h (\pi D^2 U_e N_e) \quad (5-2)$$

where $(\pi D^3 N)$ is the probability that a certain HF or DF molecule will be in contact (D being molecular hard-sphere diameter) with any other exhaust molecule (whose number density is N). When $(\pi D^3 N)$ is multiplied by hN , where h is the HF + DF molar fraction (Table 4-1), the combined term reads as the number of colliding HF/M pairs per unit volume. Assuming the electronegative formation cross-section is also πD^2 , the factor $\pi D^2 U_e N_e$ where U_e and N_e are electron velocity and number density, renders the expression for electronegative generation rate per unit volume. We note that \bar{C}_r cancels out in deriving Eq. (5-2), so that \dot{N}^- does not depend on temperature. This supports the use of the kinetic approximation in regions of continuum breakdown (plume fringes are such regions).

How is the relative magnitude of \dot{N}^- decided? To do that we multiply \dot{N}^- by $\lambda = 1/\pi D^2 N$, which is the mean free path for a fast moving particle that penetrates the plume. This expression is justified by the fact that most incident particles do collide within a distance of order λ , and when the particles are plasma ions, electrons will adhere to ion spatial distribution by virtue of the small Debye length (smaller than λ). Thus, $\lambda \dot{N}^-$ is the rate of electronegative ion generation per unit area of plume boundary. The ratio β^- between this rate and the incident electron flux is :

$$\beta^- = \lambda \dot{N}^- / N_e U_e = (\pi D^3 N) h = 2.2 \times 10^{-10} \quad (5-3)$$

where $N = 2 \times 10^{19} \text{ (m}^{-3}\text{)}$ which corresponds to Mach number $M = 30$ in the typical case (Table 4-1). The fraction of electron flux captured by HF and DF exhaust molecules to form electronegative ions is so small (due to the pair-formation term $(\pi D^3 N)$), that it cannot appreciably alter the charging flux distribution at the spacecraft surface.

Another possible effect is the recoil of HF^- or DF^- that occurs due to energy released in the electronegative formation reaction. The recoiling species might conceivably reach the surface and contaminate it. The magnitude of the recoil flux is certainly no larger than $\beta^- U_e N_e = 1300 \text{ (m}^{-2} \text{ sec}^{-1}\text{)}$, where we assume the worst case flux : $N_e = 10^{12}$, $U_e = 6 \times 10^5 \text{ (m/sec)}$ which corresponds to about 1 eV energy per electron. This flux level is about 3×10^{-13} monolayers of HF^- and DF^- per hour, so that its contribution to surface contamination is utterly negligible.

The second kind of charging effects (item (b) above) is due to the fact that the exhaust plume is impenetrable to ambient plasma (within a range of sufficiently small distance from the spacecraft, so that no extensive diluting of the plume has taken place). The downstream half of the spacecraft in oblique attitude will be in the "shadow" with respect to incident plasma. As a first approximation we may assume zero plasma flux at the shadowed surface. More accurately, this portion of the spacecraft will be subject to a plasma wake flow. However, it is quite difficult to determine the charging phenomena that take place in such a wake, as indicated by a recent work on solar sails in LEO [9]. Thus, a zero flux at the downstream half seems a practical design assumption.

Can adverse charging effects occur as a result of shadowing the downstream half? This question can be discussed only qualitatively. The reason is that a quantitative analysis requires a lumped-circuit model of the spacecraft external surface [10]. Since such a concrete design is not available, we can only discuss this question qualitatively. Obviously, assuming zero flux to the downstream half during the envisioned 5 minutes of laser firing duration, and requiring that no appreciable voltages between the two halves will evolve, leads to the stipulation that the equivalent-circuit $\text{Capacitance} \times \text{Resistance}$ should be much smaller than the firing duration.

6. CONCLUDING REMARKS

Our major quantitative conclusion is that for the relatively high ambient density assumed ($N_A = 1 \times 10^{16}$ molecules/m³ which represents Sunspot Maximum at about 200 km) and for the typical HF/DF laser exhaust (Table 4-1), the HF+DF flux backscattered by ambient molecules is several hundred monolayers per hour. This flux level may seem as not outright negligible. However, since ambient scattering flux is proportional to ambient density, it will be scaled down considerably at the lower ambient densities of higher orbital altitudes.

The operational scenario for HF/DF laser envisions 4 or 5 minutes total operating time; hence the contamination by ambient scattering may not be serious due to short operating time.

The effects of laser exhaust plume on spacecraft charging in the ionosphere were examined. It was concluded that the rate of electronegative (HF^- and DF^-) production by impinging electrons was negligible; the low rate is a consequence of the assumption that a third body is required to interact simultaneously with the HF^+ or DF^+ pair. No significant modification of charging pattern is anticipated. However, at oblique orbital attitudes, the downstream half of the spacecraft will be shadowed from the oncoming ambient plasma. This fact has to be reckoned with in designing a ring-symmetric laser spacecraft.

The emphasis in this work was on the method rather than on results. The first-collision model was demonstrated to be simple to implement in a code. It is considerably simpler than the more general and potentially more accurate Monte Carlo methods commonly used for simulating rarefied flows (8). We found out that the molecular collision model was all important in determining the return flux level, which is hardly surprising for scattering by single collision. For the same reason, the collision model would also be dominant in a Monte Carlo simulation of the ambient scattering process.

If and when a mathematical accuracy of the first-collision approximation is established for hard-spheres, it might be possible to determine a realistic collision model by comparing computed results with measurements.

This accuracy may be established in either of two ways. One way is by comparison with accurate Monte Carlo computations (using hard-spheres collision model). The other is to seek an estimate of the error incurred by considering just first collisions and ignoring all subsequent ones. This might be achieved by accounting for second collisions in an extended first-collision model, provided a simplified

scheme that will obviate the need for increase in the dimensions of the numerical flux integration can be devised. We are currently considering such second-collision approaches.

7. REFERENCES

- [1] Bird, G. A., "Breakdown of Continuum Flow in Free Jets and Rocket Plumes", Proceedings of 12th Symposium on Rarefied Gas Dynamics. In Volume 74, Progress in Aeronautics and Astronautics, Part II, pp.681, Sam S. Fisher, Editor. Published by AIAA, 1981.
- [2] Falcovitz, J., "Analytic and Numerical Computation of Ring-Symmetric Spacecraft Exhaust Plumes", Report NPS72-86-003CR, Dec. 1986, Naval Postgraduate School, Monterey, CA 93943.
- [3] Liepmann, H. W. and Roshko, A., *Elements of Gasdynamics*, John Wiley, New York, 1957.
- [4] Johnson, F. S., *Satellite Environment Handbook*, Second Edition, Stanford University Press, Stanford, California, 1965.
- [5] Mastrup, F., Broadwell, E., Miller, J. and Jacobs, T. A., "Hydrogen Fluoride Laser Technology Study", Technical Report AFWL-TR-72-28, October 1972.
- [6] Falcovitz, J., "Transient Reactive Exhaust Flow from a Ring-Symmetric HF/DF Space Laser", Report NPS72-87-002CR, Mar. 1987, Naval Postgraduate School, Monterey, CA 93943.
- [7] Falcovitz, J., "Numerical Computation of Ring-Symmetric Spacecraft Exhaust Plumes", Report NPS72-87-001CR, Jan. 1987, Naval Postgraduate School, Monterey, CA 93943.
- [8] Bird, G. A., *Molecular Gas Dynamics*, Clarendon Press, Oxford, 1976.
- [9] Hill, J. R., and Whipple, E. C., "Charging of Large Structures in Space with Application to the Solar Sail Spacecraft (survey)", *Journal of Spacecrafts and Rockets*, Vol. 22, pp. 245-253, 1985.

- [10] Garrett, H. B., "Spacecraft Charging : A Review" , pp. 167-226, in *Space Systems and Their Interactions with Earth's Environment*, Henry B. Garrett and Charles P. Pike, editors, Vol. 71 "Progress in Astronautics and Aeronautics", Published by AIAA, 1980.

APPENDIX A. DESCRIPTION OF AMB CODE

A.1 Description of Subroutines

We provide a list of the subroutines in the ambient flux integration code AMB for ring-symmetric cylindrical spacecrafts. Each subroutine is briefly described. Statements are identified by the FORTRAN statement number (columns 1 through 5).

MAIN PROGRAM The 300 loop is intended to enable several (NCASE) reruns with various data in each, all in a single run. Upon calling INIDAT1, parameters depending on data defined in INIDAT are re-computed. The 200 loop is over various XSV(NX) target points. In the 20 loop the flux integration begins: FLUXC is for particle flux and FLXU2C is for the rms of velocity of return flux molecules. All the MAX suffixed parameters denote values at which the integrand had the largest value.

The actual flux integration commences at statement 1 for the summation over strips of constant RF. This summation is terminated when convergence is attained (to within EPSR). The inner loop 2 is over azimuth angle PHI. Note that the target points are generally not in the plane of incidence (PHIA.NE.0), so that no symmetry can be assumed in the PHI integration, and it is performed twice in order to cover the entire range in PHI (IPAR=1 for PHI.GT.0, IPAR=2 for PHI.LT.0). The flux integration along the line-of-sight is done by calling FLUX.

INIDAT Initialization of data. There is no input file for this code. INIDAT1 is for parameters computed from the data defined by calling INIDAT.

SOF Stopping routine, called when an error is detected. Here we also trigger a system error by computing DSQRT(-1), in order to obtain a calling sequence printout by the operating system.

FLUX This routine calls SUMT for flux integration of one exhaust species at a time.

LIMIT Here we compute the point of intersection of the line-of-sight with the leading characteristic cone. If they do not intersect, the distance of the intersecting point TLIM is set to a very large number.

SUMT This is the line-of-sight integration routine. Runge-Kutta scheme is used (even though an explicit integral is computed). Note that ETAK and ETAIK have to be computed through a separate integration at each point of the line-of-sight integration. The integration step DT ($T = S/RF$) is re-adjusted at each integration step. The integration is terminated when convergence is attained (to within EPST).

FETA Here the integrand for the line-of-sight flux integration is evaluated. The hard-spheres collision model is used to determine the post-collision directional distribution factor PIK. The flux-average of any variable (such as UIK^{**2} in present version), can be computed by summing it multiplied by flux and subsequently dividing by the total arriving flux (see loop 31 in MAIN PROGRAM).

PATHIK Here the molecular thickness ETAIK of the I exhaust species scattered by the K ambient molecule, is computed by integration along the line-of-sight.

FT This routine computes the integrand for the ETAIK integration in PATHIK.

PATHK The analog to PATHIK for K ambient molecule. TAU is the normalized integration variable along the trajectory of the penetrating ambient molecule. Note that SHADOW=.TRUE. when the trajectory passes through the cylindrical spacecraft surface before entering the fan.

FTAU Computes the integrand for the ETAK integration in PATHK.

FAN Computes the fan coordinates PSI, XP, YP for a point on the line-of-sight. It is used to determine the Mach number and flow angle from the power-law approximation (see MATCH).

FANT Computes the fan coordinates PSI, XP, YP for a point on the ambient molecule trajectory.

HMSET Prepares the vector H MV(I) which is the value of the H(M) integral at a set of Mach number values (equally spaced in inverse Mach number). This vector is used to compute H(M) for an arbitrary M (see HINTER), since this function is needed in the power-law approximation of flow in a ring-symmetric fan. Subsequent routines MFUNC, HINTER, MATCH and AREAF are all used to implement this approximation.

MFUNC Computes the integrand for the $H(M)$ integration in HMSET.

HINTER Computes $H(M)$ for a given M , from $HMV(I)$ by linear interpolation. Note that the interpolation is done with inverse Mach number as the independent variable.

MATCH Here the approximation to the "inverse problem" of finding the Mach number at a single point in the ring-fan is implemented. An iteration scheme is used to determine the fan characteristic passing through the given point [2] .

AREAF Mach number is computed from value of area ratio function. Newton-Raphson iterations are used.

A.2 Listing of AMB code

```

C$OPTIONS LIST
C AMBIENT. SCATTERING FROM A RING PLUME BY AMBIENT AIR.
IMPLICIT REAL*8(A-H,O-Z)
COMMON /GAMA/G,G1,G2,G3,G4,G5,G6,G7,G8,G9,G10,G11,G12,G13,G14,G15,
1      G16,G17,G18,G19,G20
COMMON /PAR/CO,ENO,EMI,D,SIGMA,TLIM,DR0,EL0,Q0,T0,FACT,ALOGF,
1      DPSI0,DTMAX,DETA0,ETALIM,XSI,XSF
COMMON /NPAR/NPHI,IPAR,NP,NR,NX,NXS,NS,NSPEC,NS1,NS2,NTAU0,NETA0,
1      NAMB,NCASE,ICASE,IFAN
COMMON /GEOM/APF,PAI,PAI2,W,SW,CW,BETA,SBETA,CBETA,PSI1,SPSI1,
1      CPSI1,PSIF,SPSIF,CPSIF,TPSIF,AK,SK,CK,A0,RF,XF,YF,ZF,
2      PHISO,PHIF,SPHIF,CPHIF,DYMIN,RMIN,XS,DIST,X0,Y0,Z0,
3      DY0,DEG,PSIN,ST1,CT1,OMEGX,OMEGY,OMEGZ,XSV(21)
COMMON /EPSIL/EPSETA,EPST,EPSR
COMMON /EXTREM/TEXT(5),ETAEXT(5),ETAKXT(5),PHIEXT(5),
1      PSIEXT(5),EMEXT(5),FEXT(5),WEXT(5),
2      TMAX(5),ETAKMX(5),ETAMAX(5),PSIMAX(5),
3      EMMAX(5),FMAX(5),
4      RFMAX(5),PHIFMX(5),PHIMAX(5),WMAX(5)
COMMON /COUNTS/ICONTC,ICONTT,ICNTOT,ICNTMX,IQTOT(5),ISHAD(5)
COMMON /SPEC/WAV,XC(5),WC(5),WRC(5),XNAME(5),QFC(5),QDC(5),
1      QU2C(5),FLUXC(5),OMEGA(5),FLXU2C(5),URMSC(5)
COMMON /AMBIEN/ENA,UA,PSIA,PHIA,HA(3),WA(3),
1      UAX,UAY,UAZ,AA,BA,CA,RA,XA,YA,ZA,SHADOW
COMMON /POINT/XP,YP,XCOR,YCOR
LOGICAL SHADOW
DIMENSION DSUMF(5),DSUMD(5),DSUMAX(5),DSUMU2(5)
NCASE=1
DO 300 ICASE=1,NCASE
CALL INIDAT
GO TO (301,302,303,304,305,306,307,308,309,310,
1 311,312,313,314,315,316,317,318,319,320),ICASE
301 CONTINUE
IFAN=1
NXS=3
XSI=0.1D0
GO TO 399
302 CONTINUE
PHIA=20.D0/DEG
GO TO 399
303 CONTINUE
PHIA=50.D0/DEG
GO TO 399
304 CONTINUE
PHIA=75.D0/DEG
GO TO 399
305 CONTINUE
PHIA=100.D0/DEG
GO TO 399
306 CONTINUE
PHIA=125.D0/DEG
GO TO 399
307 CONTINUE
PHIA=150.D0/DEG
GO TO 399
308 CONTINUE
PHIA=175.D0/DEG
GO TO 399
309 CONTINUE
GO TO 399
310 CONTINUE
GO TO 399
311 CONTINUE
GO TO 399
312 CONTINUE
GO TO 399
313 CONTINUE
GO TO 399
314 CONTINUE
GO TO 399
315 CONTINUE
GO TO 399

```

316	CONTINUE	AMB0073
	GO TO 399	AMB0074
317	CONTINUE	AMB0075
	GO TO 399	AMB0076
318	CONTINUE	AMB0077
	GO TO 399	AMB0078
319	CONTINUE	AMB0079
	GO TO 399	AMB0080
320	CONTINUE	AMB0081
	GO TO 399	AMB0082
399	CONTINUE	AMB0083
	PRINT 101	AMB0084
101	FORMAT('1')	AMB0085
C		AMB0086
	CALL INDAT1	AMB0087
C		AMB0088
	DO 200 NX=1,NXS	AMB0089
	XS=XSV(NX)	AMB0090
C	(X0,Y0,Z0) IS THE POINT AT WHICH FLUX AND DENSITY ARE COMPUTED.	AMB0091
C	THE NORMAL TO THE SURFACE AT (X0,Y0,Z0) IS PARALLEL TO Y-AXIS.	AMB0092
	X0=XS	AMB0093
	Y0=A0	AMB0094
	Z0=0.	AMB0095
	DO 20 NS=NS1,NS2	AMB0096
	FLUXC(NS)=0.	AMB0097
	FLXU2C(NS)=0.	AMB0098
	OMEGA(NS)=0.	AMB0099
	DSUMAX(NS)=0.	AMB0100
	IQTOT(NS)=0	AMB0101
	ISHAD(NS)=0.	AMB0102
	TMAX(NS)=-1.D 44	AMB0103
	ETAKMX(NS)=-1.D 44	AMB0104
	PHIMAX(NS)=-1.D 44	AMB0105
	PHIFMX(NS)=-1.D 44	AMB0106
	WMAX(NS)=-1.D 44	AMB0107
	PSIMAX(NS)=-1.D 44	AMB0108
	ETAMAX(NS)=-1.D 44	AMB0109
	RFMAX(NS)=-1.D 44	AMB0110
	EMMAX(NS)=-1.D 44	AMB0111
	FMAX(NS)=-1.D 44	AMB0112
20	CONTINUE	AMB0113
	RN=RMIN	AMB0114
	APF=A0-0.5D0*DR0*SPSIF	AMB0115
	NR=0	AMB0116
1	NR=NR+1	AMB0117
	DR=DR0	AMB0118
	DR=DR0*(APF/A0)	AMB0119
C	DR=DR0*(1.D0+0.4D0*DR0/XS)**NR	AMB0120
	RF=RN+DR/2.D0	AMB0121
	APF=A0+RF*SPSIF	AMB0122
	PHISOF=DACOS(A0/APF)	AMB0123
C	DPHI0=0.1D0	AMB0124
C	NPHI=PHISOF/DPHI0+2	AMB0125
	DPHI=PHISOF/DBLE(NPHI)	AMB0126
	DO 21 NS=NS1,NS2	AMB0127
	DSUMF(NS)=0.	AMB0128
	DSUMU2(NS)=0.	AMB0129
	DSUMD(NS)=0.	AMB0130
21	CONTINUE	AMB0131
	DOMEGR=0.	AMB0132
	DO 2 NP=1,NPHI	AMB0133
	DO 2 IPAR=1,2	AMB0134
	PHIF=(DBLE(NP)-0.5D0)*DPHI	AMB0135
	IF(IPAR.EQ.2) PHIF=-PHIF	AMB0136
C		AMB0137
	CALL FLUX	AMB0138
C		AMB0139
	CROSS1=OMEGY	AMB0140
	CROSS2=(SPSIF)*(-OMEGX)+(-CPSIF*CPHIF)*(-OMEGY)+	AMB0141
1	(-CPSIF*SPHIF)*(-OMEGZ)	AMB0142
	IF(CROSS1.LE.0.)	AMB0143
	1CALL SOF('DIRECTION COSINE OF SURFACE NORMAL SHOULD BE POSITIVE')	AMB0144

```

IF(CROSS2.LE.0.)
1CALL SOF('NORMAL TO LIMITING CONE HAS NEGATIVE PROJECTION ON LINE-
1OF-SIGHT')
DOMEGR=CROSS2*DPHI*APF*DR/DIST**2
DOMEGR=DOMEGR+DOMEGR
DO 24 NS=NS1,NS2
DSUMF(NS)=DSUMF(NS)+DOMEGR*QFC(NS)*CROSS1
DSUMU2(NS)=DSUMU2(NS)+DOMEGR*QU2C(NS)*CROSS1
IF(DSUMAX(NS).GT.DOMEGR*QFC(NS)*CROSS1) GO TO 24
DSUMAX(NS)=DOMEGR*QFC(NS)*CROSS1
TMAX(NS)=TEXT(NS)
ETAKMX(NS)=ETAKXT(NS)
PHIMAX(NS)=PHIEXT(NS)*DEG
PHIFMX(NS)=PHIF*DEG
WMAX(NS)=WEXT(NS)*DEG
PSIMAX(NS)=PSIEXT(NS)*DEG
ETAMAX(NS)=ETAEXT(NS)
RFMAX(NS)=RF
EMMAX(NS)=EMEXT(NS)
FMAX(NS)=QFC(NS)*XC(NS)*Q0
24 CONTINUE
2 CONTINUE
DO 26 NS=NS1,NS2
FLUXC(NS)=FLUXC(NS)+DSUMF(NS)
FLXU2C(NS)=FLXU2C(NS)+DSUMU2(NS)
OMEGA(NS)=OMEGA(NS)+DOMEGR
26 CONTINUE
RN=RN+DR
IF(NR.LE.2) GO TO 1
IF(NR.GT.99) GO TO 10
DO 27 NS=NS1,NS2
IF(FLUXC(NS).EQ.0.) GO TO 27
ERR=(DSUMF(NS)/FLUXC(NS))/DOMEGR
IF(ERR.GT.EPSR) GO TO 28
27 CONTINUE
GO TO 10
28 CONTINUE
GO TO 1
10 CONTINUE
DO 31 NS=NS1,NS2
FLUXC(NS)=XC(NS)*FLUXC(NS)*Q0
OMEGA(NS)=OMEGA(NS)/(2.D0*PAI*DCOS(PSIF/2.D0)**2)
FLXU2C(NS)=XC(NS)*FLXU2C(NS)*Q0
URMSC(NS)=0.
IF(FLUXC(NS).EQ.0.) GO TO 31
URMSC(NS)=DSQRT(FLXU2C(NS)/FLUXC(NS))
C AVERAGE EM (SEE FETA)
URMSC(NS)= FLXU2C(NS)/FLUXC(NS)
31 CONTINUE
PRINT 11,NX,NR,XS,RF,DR,PHISO*DEG
11 FORMAT(///1X,'NX,NR,XS,RF,DR,PHISO=' ,2I4,3D13.4,F8.4,
1 3X,'FLUX AND EXTREMA VALUES, ALL SPECIES:'/)
PRINT 12
12 FORMAT(/1X,' NAME ', ' IQTOT', ' ISHAD',
1 ' FMAX ', ' OMEGA', ' TMAX',
2 ' ETAKMX', ' ETAMAX', ' PSIMAX',
3 ' EMMAX', ' RFMAX', ' PI-WMAX',
4 ' URMSC', ' FLUXC / LOG' /)
DO 14 NS=NS1,NS2
DLF=0.
IF(FLUXC(NS).NE.0)
1DLF=DLOG10(FLUXC(NS))+100.D0+1.D-11
IDL=DLF
DLF=DLF-DBLE(IDL)
PRINT 13,XNAME(NS),IQTOT(NS),ISHAD(NS),FMAX(NS),OMEGA(NS),
1 TMAX(NS),ETAKMX(NS),ETAMAX(NS),
2 PSIMAX(NS),EMMAX(NS),RFMAX(NS),
3 180.D0-WMAX(NS),URMSC(NS),
4 FLUXC(NS),DLF
13 FORMAT(1X,A6,2I6,D10.3,4F8.4,4F8.1,F8.2,D10.3,'/',F4.2)
14 CONTINUE
200 CONTINUE

```

AMB0145
 AMB0146
 AMB0147
 AMB0148
 AMB0149
 AMB0150
 AMB0151
 AMB0152
 AMB0153
 AMB0154
 AMB0155
 AMB0156
 AMB0157
 AMB0158
 AMB0159
 AMB0160
 AMB0161
 AMB0162
 AMB0163
 AMB0164
 AMB0165
 AMB0166
 AMB0167
 AMB0168
 AMB0169
 AMB0170
 AMB0171
 AMB0172
 AMB0173
 AMB0174
 AMB0175
 AMB0176
 AMB0177
 AMB0178
 AMB0179
 AMB0180
 AMB0181
 AMB0182
 AMB0183
 AMB0184
 AMB0185
 AMB0186
 AMB0187
 AMB0188
 AMB0189
 AMB0190
 AMB0191
 AMB0192
 AMB0193
 AMB0194
 AMB0195
 AMB0196
 AMB0197
 AMB0198
 AMB0199
 AMB0200
 AMB0201
 AMB0202
 AMB0203
 AMB0204
 AMB0205
 AMB0206
 AMB0207
 AMB0208
 AMB0209
 AMB0210
 AMB0211
 AMB0212
 AMB0213
 AMB0214
 AMB0215
 AMB0216

```

102 PRINT 102
300 FORMAT(///1X,'END RING RUN',///)
CONTINUE
STOP
END
SUBROUTINE INIDAT
IMPLICIT REAL*8(A-H,O-Z)
REAL*8 LAMDA0,LAMDA1
CHARACTER*8 XNAME,XNAMED
COMMON /GAMA/G,G1,G2,G3,G4,G5,G6,G7,G8,G9,G10,G11,G12,G13,G14,G15,
1 G16,G17,G18,G19,G20
COMMON /PAR/CO,ENO,EM1,D,SIGMA,TLIM,DR0,EL0,Q0,T0,FACT,ALOGF,
1 DPSI0,DTMAX,DETA0,ETALIM,XSI,XSF
COMMON /NPAR/NPHI,IPAR,NP,NR,NX,NXS,NS,NSPEC,NS1,NS2,NTAU0,NETA0,
1 NAMB,NCASE,ICASE,IFAN
COMMON /GEOM/APF,PAI,PAI2,W,SW,CW,BETA,SBETA,CBETA,PSI1,SPSI1,
1 CPSI1,PSIF,SPSIF,CPSIF,TPSIF,AK,SK,CK,A0,RF,XF,YF,ZF,
2 PHISOF,PHIF,SPHIF,CPHIF,DYMIN,RMIN,XS,DIST,X0,Y0,Z0,
3 DY0,DEG,PSIN,ST1,CT1,OMEGX,OMEGY,OMEGZ,XSV(21)
COMMON /EPSIL/EPSETA,EPST,EPSR
COMMON /EXTREM/TEXT(5),ETAEXT(5),ETAKXT(5),PHIEXT(5),
1 PSIEXT(5),EMEXT(5),FEXT(5),WEXT(5),
2 TMAX(5),ETAKMX(5),ETAMAX(5),PSIMAX(5),
3 EMMAX(5),FMAX(5),
4 RFMAX(5),PHIFMX(5),PHIMAX(5),WMAX(5)
COMMON /COUNTS/ICONTC,ICONTT,ICNTOT,ICNTMX,IQTOT(5),ISHAD(5)
COMMON /SPEC/WAV,XC(5),WC(5),WRC(5),XNAME(5),QFC(5),QDC(5),
1 QU2C(5),FLUXC(5),OMEGA(5),FLXU2C(5),URMSC(5)
COMMON /AMBIEN/ENA,UA,PSIA,PHIA,HA(3),WA(3),
1 UAX,UAY,UAZ,AA,BA,CA,RA,XA,YA,ZA,SHADOW
COMMON /POINT/XP,YP,XCOR,YCOR
LOGICAL SHADOW
DIMENSION XCD(5),WCD(5),XNAMED(5)
DATA XCD/.091D0,.091D0,.104D0,.135D0,.579D0/
DATA WCD/1.00D0,20.00D0,2.00D0,21.0D0,4.00D0/
DATA XNAMED/' H ',' HF ',' H2 ',' DF ',' HE '/
DATA IFIRST/0/
IFAN=2
PAI=4.D0*DATAN(1.D0)
PAI2=PAI/2.D0
DEG=180.D0/PAI
AR=8.3143D3
AV=6.022D 26
C OMEGAC=0.5 IS FOR HARD SPHERE COLLISIONS,
C AN AVERAGE RECOMMENDED VALUE IS ABOUT OMEGAC=0.75
OMEGAC=0.5D0
NSPEC=5
NS1=2
NS2=2
DO 51 NS=1,NSPEC
XC(NS)=XCD(NS)
WC(NS)=WCD(NS)
XNAME(NS)=XNAMED(NS)
51 CONTINUE
C COMBINE HF AND DF MOLE FRACTIONS INTO HF FRACTION
XC(2)=XC(2)+XC(4)
XC(4)=0.
C
A0=2.5D0
EM1=4.D0
RH00=0.0075D0
T0=1400.D0
G=1.54D0
D=2.5D-10
NXS=1
XSI=1.0D0
XSF=10.D0
C AMBIENT AIR
ENA=1.00D 16
UA=8.D 3
NAMB=3
WA(1)=28.D0

```

```

WA(2)=32.D0
WA(3)=16.D0
HA(1)=1.D0
HA(2)=0.
HA(3)=0.
PSIA=20.D0/DEG
PHIA=0.00D0/DEG
C INTEGRATION PARAMETERS
NPHI=6
NTAU0=4
NETA0=4
ICNTMX=100
RMIN=0.
DR0=0.10D0
DPSI0=0.20D0
DTMAX=1.0D0
DETA0=0.50D0
ETALIM=10.D0
EPST=0.5D0
EPSR=0.3D0
FACT=1.D 20
RETURN
C*****
C COMPUTATION OF DATA-DEPENDENT PARAMETERS
C*****
ENTRY INDAT1
C*****
ALOGF=DLOG(FACT)
WAV=0.
DO 52 NS=1,NSPEC
WAV=WAV+XC(NS)*WC(NS)
52 CONTINUE
DO 53 NS=1,NSPEC
WRC(NS)=WC(NS)/WAV
53 CONTINUE
SIGMA=PAI*D**2
ENO=RH00*AV/WAV
C0=DSQRT(G*AR*T0/WAV)
XSV(1)=XSI
IF(NXS.EQ.1) GO TO 12
DXL=(DLOG(XSF)-DLOG(XSI))/(DBLE(NXS)-1.D0)
XLI=DLOG(XSI)
DO 11 NX=2,NXS
XSV(NX)=DEXP(XLI+(DBLE(NX)-1.D0)*DXL)
11 CONTINUE
12 CONTINUE
G1=(G-1.D0)/2.D0
G2=(G+1.D0)/(2.D0*(G-1.D0))
G3=G/2.D0
G4=(G+1.D0)/(G-1.D0)
G5=DSQRT((G+1.D0)/(G-1.D0))
G6=1.D0/(G-1.D0)
G7=2.D0/(G+1.D0)
G8=(0.5D0*(G+1.D0)**2/(G-1.D0))*(1.D0/(G+1.D0))*
1 ((G+1.D0)/(G-1.D0))*((G-1.D0)/(G+1.D0))
G9=(G+3.D0)/(2.D0*(G-1.D0))
G10=(7.D0-3.D0*G)/(2.D0*(G-1.D0))
G11=(5.D0-3.D0*G)/(2.D0*(G-1.D0))
G13=(2.D0-G)/(2.D0*(G-1.D0))
G14=G/(2.D0*(G-1.D0))
G15=(G+1.D0)/(3.D0-G)
ZETA1=G5*DATAN(DSQRT(EM1**2-1.D0)/G5)
AMU1=DASIN(1.D0/EM1)
PSI1=PAI2+AMU1
SPSI1=DSIN(Psi1)
CPSI1=DCOS(Psi1)
PSIF=PAI2+AMU1+ZETA1-G5*PAI2
SPSIF=DSIN(PSIF)
CPSIF=DCOS(PSIF)
TPSIF=DTAN(PSIF)
TETA1=PSI1-AMU1
ST1=DSIN(TETA1)

```

```

AMB0289
AMB0290
AMB0291
AMB0292
AMB0293
AMB0294
AMB0295
AMB0296
AMB0297
AMB0298
AMB0299
AMB0300
AMB0301
AMB0302
AMB0303
AMB0304
AMB0305
AMB0306
AMB0307
AMB0308
AMB0309
AMB0310
AMB0311
AMB0312
AMB0313
AMB0314
AMB0315
AMB0316
AMB0317
AMB0318
AMB0319
AMB0320
AMB0321
AMB0322
AMB0323
AMB0324
AMB0325
AMB0326
AMB0327
AMB0328
AMB0329
AMB0330
AMB0331
AMB0332
AMB0333
AMB0334
AMB0335
AMB0336
AMB0337
AMB0338
AMB0339
AMB0340
AMB0341
AMB0342
AMB0343
AMB0344
AMB0345
AMB0346
AMB0347
AMB0348
AMB0349
AMB0350
AMB0351
AMB0352
AMB0353
AMB0354
AMB0355
AMB0356
AMB0357
AMB0358
AMB0359
AMB0360

```



```

CT1=DCOS(TETA1)
Q0=ENA*UA
LAMDA0=1.D0/(DSQRT(2.D0)*SIGMA*ENO)
LAMDA1=LAMDA0*(1.D0+G1*EM1**2)**(G6-OMEGAC+0.5D0)
AA=DCOS(PSIA)
BA=DSIN(PSIA)*DCOS(PHIA)
CA=DSIN(PSIA)*DSIN(PHIA)
UAX=-UA*AA
UAY=-UA*BA
UAZ=-UA*CA
XCOR=0.
YCOR=A0
C
PRINT 201, NSPEC, XNAME
201 FORMAT(/1X, 'SPECIES DATA   NSPEC=', I3/
1 1X, 'SPECIES NAMES       ', 11(2X, A6, 2X))
PRINT 202, XC
202 FORMAT(1X, 'MOLE FRACTION XC=', 11(F8.4, 2X))
PRINT 203, WC
203 FORMAT(1X, 'MOL. WEIGHT   WC=', 11(F8.4, 2X))
PRINT 21, AR, AV, WAV, G, RH00, T0, EN0, C0, D
21 FORMAT(/1X, 'THERMODYNAMIC DATA'/
1 1X, 'AR, AV, WAV, GAMMA=', 2X, 2D14.5, 2F9.3/
2 1X, 'RH00, T0, EN0, C0, D=', D12.4, F8.0, D13.5, 2D12.4)
PRINT 22, EM1, PSI1*DEG, PSIF*DEG,
1 A0, LAMDA0, LAMDA1
22 FORMAT(/1X, 'FLOW AND GEOMETRY DATA'/
1 1X, 'EM1, PSI1, PSIF=', 3F9.3/
2 1X, 'A0, LAMDA0, LAMDA1=', F9.3, 2D13.4)
PRINT 23, DPSI0, DTMAX, DETAO, ETALIM, DR0, RMIN,
1 EPST, EPSR,
2 NPHI, NTAU0, NETA0
23 FORMAT(/1X, 'INTEGRATION DATA'/
1 1X, 'DPSI0, DTMAX, DETAO, ETALIM=', 4F9.4/
2 1X, 'DR0, RMIN, =', 2D13.4/
3 1X, 'EPST, EPSR=', 2D12.3/
4 1X, 'NPHI, NTAU0, NETA0=', 3I6)
PRINT 24, ENA, UA, PSIA*DEG, PHIA*DEG
24 FORMAT(/1X, 'ABBREVIATED AIR DATA'/
1 1X, 'ENA, UA=', 2D13.4/
2 1X, 'PSIA, PHIA=', 2F9.1)
GO TO (251, 252), IFAN

251 CONTINUE
PRINT 2510, IFAN
2510 FORMAT(/1X, 'RING-FAN APPROXIMATED AS PLANAR.   IFAN=', I4)
GO TO 250
252 CONTINUE
PRINT 2520, IFAN
2520 FORMAT(/1X, 'RING-FAN APPROXIMATED BY MATCHED APPROXIMATION.',
1 4X, 'IFAN=', I4)
250 CONTINUE
PRINT 29
29 FORMAT(///1X, 'END DATA'///)
IF(IFIRST.EQ.0.AND.IFAN.EQ.2)
1CALL HMSET
IF(IFAN.EQ.2) IFIRST=IFIRST+1
RETURN
END
C$OPTIONS LIST
SUBROUTINE SOF(ISTOP)
IMPLICIT REAL*8(A-H, O-Z)
CHARACTER*4 ISTOP(1)
COMMON /GAMA/G, G1, G2, G3, G4, G5, G6, G7, G8, G9, G10, G11, G12, G13, G14, G15,
1 G16, G17, G18, G19, G20
COMMON /PAR/C0, EN0, EM1, D, SIGMA, TLIM, DR0, ELO, Q0, T0, FACT, ALOGF,
1 DPSI0, DTMAX, DETAO, ETALIM, XSI, XSF
COMMON /NPAR/NPHI, IPAR, NP, NR, NX, NXS, NS, NSPEC, NS1, NS2, NTAU0, NETA0,
1 NAMB, NCASE, ICASE, IFAN
COMMON /GEOM/APF, PA1, PA12, W, SW, CW, BETA, SBETA, CBETA, PSI1, SPSI1,
1 CPSI1, PSIF, SPSIF, CPSIF, TPSIF, AK, SK, CK, A0, RF, XF, YF, ZF,
2 PHISOF, PHIF, SPHIF, CPHIF, DYMIN, RMIN, XS, DIST, X0, Y0, Z0,

```

```

3          DY0, DEG, PSIN, ST1, CT1, OMEGX, OMEGY, OMEGZ, XSV(21)      AMB0433
COMMON /EPSIL/EPSETA, EPST, EPSR                                       AMB0434
COMMON /EXTREM/TEXT(5), ETAEXT(5), ETAKXT(5), PHIEXT(5),              AMB0435
1          PSIEXT(5), EMEXT(5), FEXT(5), WEXT(5),                      AMB0436
2          TMAX(5), ETAKMX(5), ETAMAX(5), PSIMAX(5),                  AMB0437
3          EMMAX(5), FMAX(5),                                          AMB0438
4          RFMAX(5), PHIFMX(5), PHIMAX(5), WMAX(5)                    AMB0439
COMMON /SOFPR/C, DSUMF, DSUMD, T, ETA, DETA, SUM, DSUM, SUMU, DSUMU    AMB0440
COMMON /SUMS/SUMF(5), SUMD(5), SUMU2(5)                                AMB0441
COMMON /COUNTS/ICONTC, ICONTT, ICNTOT, ICNTMX, IQTOT(5), ISHAD(5)    AMB0442
COMMON /SPEC/WAV, XC(5), WC(5), WRC(5), XNAME(5), QFC(5), QDC(5),      AMB0443
1          QU2C(5), FLUXC(5), OMEGA(5), FLXU2C(5), URMSC(5)          AMB0444
1 PRINT 1, ISTOP                                                         AMB0445
1 FORMAT(///1X, 2H**, 2X, 30A4, 2X, 2H**, ///)                         AMB0446
71 PRINT 71, NS, NP, NR, NX, ICONTC, ICONTT                             AMB0447
71 FORMAT(1X, 'NS, NP, NR, NX, ICONTC, ICONTT=', 6I6/)                 AMB0448
IF(NS.GT.NSPEC) NS=1                                                    AMB0449
72 PRINT 72, RF, PHIF*DEG, PHISO*DEG, W*DEG, BETA*DEG                 AMB0450
72 FORMAT(1X, 'RF, PHIF, PHISO, W, BETA=', D14.5, 4F10.3/)           AMB0451
72 PRINT 73, C, T, TLIM, ETA                                           AMB0452
73 FORMAT(1X, 'C, T, TLIM, ETA=', 4D14.5/)                             AMB0453
73 PRINT 74, DSUM, SUM, DSUMF, SUMF(NS), SUMD(NS), QDC(NS), QFC(NS),    AMB0454
1          FLUXC(NS), OMEGA(NS)                                         AMB0455
74 FORMAT(1X, 'DSUM, SUM, DSUMF, SUMF(NS), SUMD(NS)=', 5D14.5/        AMB0456
1          1X, 'QDC(NS), QFC(NS), FLUXC(NS), OMEGA(NS)=', 4D14.5/)    AMB0457
XX=-1.D0                                                                AMB0458
YY=DSQRT(XX)+1.D0                                                       AMB0459
STOP                                                                    AMB0460
END                                                                      AMB0461
SUBROUTINE FLUX                                                         AMB0462
IMPLICIT REAL*8(A-H, O-Z)                                              AMB0463
COMMON /GAMA/G, G1, G2, G3, G4, G5, G6, G7, G8, G9, G10, G11, G12, G13, G14, G15, AMB0464
1          G16, G17, G18, G19, G20                                     AMB0465
COMMON /PAR/C0, EN0, EM1, D, SIGMA, TLIM, DR0, EL0, Q0, T0, FACT, ALOGF, AMB0466
1          DPSI0, DTMAX, DETA0, ETALIM, XSI, XSF                     AMB0467
COMMON /NPAR/NPHI, IPAR, NP, NR, NX, NXS, NS, NSPEC, NS1, NS2, NTAU0, NETA0, AMB0468
1          NAMB, NCASE, ICASE, IFAN                                   AMB0469
COMMON /GEOM/APF, PAI, PAI2, W, SW, CW, BETA, SBETA, CBETA, PSI1, SPSI1, AMB0470
1          CPSI1, PSIF, SPSIF, CPSIF, TPSIF, AK, SK, CK, A0, RF, XF, YF, ZF, AMB0471
2          PHISO, PHIF, SPHIF, CPHIF, DYMIN, RMIN, XS, DIST, X0, Y0, Z0, AMB0472
3          DY0, DEG, PSIN, ST1, CT1, OMEGX, OMEGY, OMEGZ, XSV(21)    AMB0473
COMMON /EPSIL/EPSETA, EPST, EPSR                                       AMB0474
COMMON /EXTREM/TEXT(5), ETAEXT(5), ETAKXT(5), PHIEXT(5),              AMB0475
1          PSIEXT(5), EMEXT(5), FEXT(5), WEXT(5),                      AMB0476
2          TMAX(5), ETAKMX(5), ETAMAX(5), PSIMAX(5),                  AMB0477
3          EMMAX(5), FMAX(5),                                          AMB0478
4          RFMAX(5), PHIFMX(5), PHIMAX(5), WMAX(5)                    AMB0479
COMMON /SOFPR/C, DSUMF, DSUMD, T, ETA, DETA, SUM, DSUM, SUMU, DSUMU    AMB0480
COMMON /COUNTS/ICONTC, ICONTT, ICNTOT, ICNTMX, IQTOT(5), ISHAD(5)    AMB0481
COMMON /SPEC/WAV, XC(5), WC(5), WRC(5), XNAME(5), QFC(5), QDC(5),      AMB0482
1          QU2C(5), FLUXC(5), OMEGA(5), FLXU2C(5), URMSC(5)          AMB0483
COMMON /SUMS/SUMF(5), SUMD(5), SUMU2(5)                                AMB0484
ELO=SIGMA*RF*EN0                                                        AMB0485
IF(Z0.NE.0.)                                                            AMB0486
1CALL SOF('THE SCHEME HERE IS NOT WRITTEN FOR Z0.NE.0.')
```

```

W=PAI2-DATAN(CW/SW)
OMEGX=CW
OMEGY=SW*CBETA
OMEGZ=SW*SBETA
CALL LIMIT
C
DO 20 NS=NS1,NS2
SUMF(NS)=0.
SUMU2(NS)=0.
SUMD(NS)=0.
FEXT(NS)=0.
CALL SUMT
SUMF(NS)=SUM
SUMU2(NS)=SUMU
QFC(NS)=SUMF(NS)/FACT
QU2C(NS)=SUMU2(NS)/FACT
FEXT(NS)=FEXT(NS)/FACT
CALL FAN(TEXT(NS),PSIEXT(NS),PHIEXT(NS))
IF(PSIEXT(NS).LT.PSIF-1.D-10) CALL SOF('PSIEXT(NS).LT.PSIF')
IF(PSIEXT(NS).GT.PSI1) PSIEXT(NS)=PSI1
PSI0=PSIEXT(NS)
T=TEXT(NS)
CALL MATCH(T,PSI0,EM,TETA)
EMEXT(NS)=EM
WEXT(NS)=W
IQTOT(NS)=IQTOT(NS)+ICONTT
20 CONTINUE
RETURN
END
SUBROUTINE LIMIT
IMPLICIT REAL*8(A-H,O-Z)
COMMON /GAMA/G,G1,G2,G3,G4,G5,G6,G7,G8,G9,G10,G11,G12,G13,G14,G15,
1 G16,G17,G18,G19,G20
COMMON /PAR/CO,ENO,EM1,D,SIGMA,TLIM,DR0,EL0,Q0,T0,FACT,ALOGF,
1 DPSI0,DTMAX,DETA0,ETALIM,XSI,XSF
COMMON /NPAR/NPHI,IPAR,NP,NR,NX,NXS,NS,NSPEC,NS1,NS2,NTAU0,NETA0,
1 NAMB,NCASE,ICASE,IFAN
COMMON /GEOM/APF,PAI,PAI2,W,SW,CW,BETA,SBETA,CBETA,PSI1,SPSI1,
1 CPSI1,PSIF,SPSIF,CPSIF,TPSIF,AK,SK,CK,A0,RF,XF,YF,ZF,
2 PHISO,PHIF,SPHIF,CPHIF,DYMIN,RMIN,XS,DIST,X0,Y0,Z0,
3 DY0,DEG,PSIN,ST1,CT1,OMEGX,OMEGY,OMEGZ,XSV(21)
COMMON /EPSIL/EPSETA,EPST,EPSR
COMMON /EXTREM/TEXT(5),ETAEXT(5),ETAKXT(5),PHIEXT(5),
1 PSIEXT(5),EMEXT(5),FEXT(5),WEXT(5),
2 TMAX(5),ETAKMX(5),ETAMAX(5),PSIMAX(5),
3 EMMAX(5),FMAX(5),
4 RFMAX(5),PHIFMX(5),PHIMAX(5),WMAX(5)
COMMON /SPEC/WAV,XC(5),WC(5),WRC(5),XNAME(5),QFC(5),QDC(5),
1 QU2C(5),FLUXC(5),OMEGA(5),FLXU2C(5),URMSC(5)
AAA=(CW/CPSI1)**2-1.D0
IF(AAA.LT.1.D-10) GO TO 1
TPSI1=SPSI1/CPSI1
AP1=A0+XF*TPSI1
BBB=2.D0*(AP1*CW*TPSI1-SW*APF*(CBETA*CPHIF+SBETA*SPHIF))
CCC=AP1**2-APF**2
DDD=BBB**2-4.D0*AAA*CCC
TLIM=(-BBB+DSQRT(DDD))/(2.D0*AAA)
TLIM=TLIM/RF
RETURN
1 CONTINUE
TLIM=1.D 55
RETURN
END
SUBROUTINE SUMT
IMPLICIT REAL*8(A-H,O-Z)
COMMON /GAMA/G,G1,G2,G3,G4,G5,G6,G7,G8,G9,G10,G11,G12,G13,G14,G15,
1 G16,G17,G18,G19,G20
COMMON /PAR/CO,ENO,EM1,D,SIGMA,TLIM,DR0,EL0,Q0,T0,FACT,ALOGF,
1 DPSI0,DTMAX,DETA0,ETALIM,XSI,XSF
COMMON /NPAR/NPHI,IPAR,NP,NR,NX,NXS,NS,NSPEC,NS1,NS2,NTAU0,NETA0,
1 NAMB,NCASE,ICASE,IFAN
COMMON /GEOM/APF,PAI,PAI2,W,SW,CW,BETA,SBETA,CBETA,PSI1,SPSI1,

```

```

1      CPSI1,PSIF,SPSIF,CPSIF,TPSIF,AK,SK,CK,A0,RF,XF,YF,ZF,AMB0577
2      PHISO,PHIF,SPHIF,CPHIF,DYMIN,RMIN,XS,DIST,X0,Y0,Z0,AMB0578
3      DY0,DEG,PSIN,ST1,CT1,OMEGX,OMEGY,OMEGZ,XSV(21)AMB0579
COMMON /EPSIL/EPSETA,EPST,EPSR      AMB0580
COMMON /EXTREM/TEXT(5),ETAEXT(5),ETAKXT(5),PHIEXT(5),      AMB0581
1      PSIEXT(5),EMEXT(5),FEXT(5),WEXT(5),      AMB0582
2      TMAX(5),ETAKMX(5),ETAMAX(5),PSIMAX(5),      AMB0583
3      EMMAX(5),FMAX(5),      AMB0584
4      RFMAX(5),PHIFMX(5),PHIMAX(5),WMAX(5)      AMB0585
COMMON /SOFPR/CC,DSUMF,DSUMD,T,ETA,DETA,SUM,DSUM,SUMU,DSUMU      AMB0586
COMMON /COUNTS/ICNTC,ICNTT,ICNTOT,ICNTMX,IQTOT(5),ISHAD(5)      AMB0587
COMMON /SPEC/WAV,XC(5),WC(5),WRC(5),XNAME(5),QFC(5),QDC(5),      AMB0588
1      QU2C(5),FLUXC(5),OMEGA(5),FLXU2C(5),URMSC(5)      AMB0589
COMMON /SUMS/SUMF(5),SUMD(5),SUMU2(5)      AMB0590
C  INTEGRATION OF FLUX ARRIVING ALONG A SINGLE RAY      AMB0591
  DT=DPSI0      AMB0592
  PSIN=PSIF      AMB0593
  ETA1=0.      AMB0594
  ETA3=0.      AMB0595
  FETA4=0.      AMB0596
  FETAU4=0.      AMB0597
  T=0.      AMB0598
  SUM=0.      AMB0599
  SUMU=0.      AMB0600
  ICNTT=0      AMB0601
1  ICNTT=ICNTT+1      AMB0602
  PSIL=PSIN      AMB0603
  DT2=DT/2.D0      AMB0604
  DT6=DT/6.D0      AMB0605
  T1=T+DT2      AMB0606
  T2=T+DT      AMB0607
  FETA1=FETA4      AMB0608
  FETAU1=FETAU4      AMB0609
  CALL PATHK(T1,ETAK1)      AMB0610
  CALL FETA(T1,ETA1,ETAK1,GT2,FETA2,FETAU2)      AMB0611
  FETA3=FETA2      AMB0612
  FETAU3=FETAU2      AMB0613
  CALL PATHK(T2,ETAK3)      AMB0614
  CALL FETA(T2,ETA3,ETAK3,GT4,FETA4,FETAU4)      AMB0615
  DETA=DT*GT4      AMB0616
  DSUM=DT6*(FETA1+2.D0*(FETA2+FETA3)+FETA4)      AMB0617
  DSUMU=DT6*(FETAU1+2.D0*(FETAU2+FETAU3)+FETAU4)      AMB0618
  T=T+DT      AMB0619
  ETA=ETA3      AMB0620
  ETAK=ETAK3      AMB0621
  SUM=SUM+DSUM      AMB0622
  SUMU=SUMU+DSUMU      AMB0623
  IF(FEXT(NS).GT.FETA4) GO TO 10      AMB0624
  FEXT(NS)=FETA4      AMB0625
  TEXT(NS)=T      AMB0626
  ETAEXT(NS)=ETA      AMB0627
  ETAKXT(NS)=ETAK      AMB0628
10  CONTINUE      AMB0629
C  STEP CONTROL (DT)      AMB0630
  CALL FAN(T,PSI,PHI)      AMB0631
  IF(PSI.LT.PSIF-1.D-10) CALL SOF('PSI.LT.PSIF')      AMB0632
  IF(PSI.GT.PSI1) PSI=PSI1      AMB0633
  PSIN=PSI      AMB0634
  DPSI=PSIN-PSIL      AMB0635
  DTP=DT*(DPSI0/(DPSI+1.D-10))      AMB0636
  DTE=DT*(DETA0/(DETA+1.D-10))      AMB0637
  DT1=1.2D0*DT      AMB0638
  DT=DMIN1(DTP,DTE,DT1,DTMAX)      AMB0639
  IF(DT.LE.0.) CALL SOF('COMPUTED DT NEGATIVE')      AMB0640
15  CONTINUE      AMB0641
  IF(IPAR.LT.1)      AMB0642
1  PRINT 111,NR,NP,T,PSI*DEG,PHI*DEG,ETA,ETAK,SUM,DSUM/(SUM+1.D-20)      AMB0643
111  FORMAT(1X,'NR,NP,T,PSI,PHI=',2I3,3D12.3/      AMB0644
1      1X,'ETA,ETAK,SUM,ERRR=',4D12.3)      AMB0645
  IF(ICNTT.GT.ICNTMX)      AMB0646
1  CALL SOF('ICNTT TOO LARGE')      AMB0647
  IF(ICNTT.LE.2) GO TO 1      AMB0648

```

```

IF(ETA+ETAK.GT.ETALIM) GO TO 100
IF(T.GT.50.D0 .OR. T*RF.GT.A0) GO TO 100
IF(SUM.EQ.0.) GO TO 1
ERR=(DSUM/SUM)/DT
100 IF(ERR.GT.EPST) GO TO 1
CONTINUE
SUM=SUM*ELO
SUMU=SUMU*ELO
RETURN
END
SUBROUTINE FETA(T,ETAIK,ETAK,GT,FET,FETU2)
IMPLICIT REAL*8(A-H,O-Z)
REAL*8 MU1,MU2
COMMON /GAMA/G,G1,G2,G3,G4,G5,G6,G7,G8,G9,G10,G11,G12,G13,G14,G15,
1 G16,G17,G18,G19,G20
COMMON /PAR/CO,ENO,EM1,D,SIGMA,TLIM,DR0,ELO,Q0,T0,FACT,ALOGF,
1 DPSI0,DTMAX,DETA0,ETALIM,XSI,XSF
COMMON /NPAR/NPHI,IPAR,NP,NR,NX,NXS,NS,NSPEC,NS1,NS2,NTAU0,NETA0,
1 NAMB,NCASE,ICASE,IFAN
COMMON /GEOM/APF,PAI,PAI2,W,SW,CW,BETA,SBETA,CBETA,PSI1,SPSI1,
1 CPSI1,PSIF,SPSIF,CPSIF,TPSIF,AK,SK,CK,A0,RF,XF,YF,ZF,
2 PHISO,PHIF,SPHIF,CPHIF,DYMIN,RMIN,XS,DIST,X0,Y0,Z0,
3 DY0,DEG,PSIN,ST1,CT1,OMEGX,OMEGY,OMEGZ,XSV(21)
COMMON /EPSIL/EPSETA,EPST,EPSR
COMMON /EXTREM/TEXT(5),ETAEXT(5),ETAKXT(5),PHIEXT(5),
1 PSIEXT(5),EMEXT(5),FEXT(5),WEXT(5),
2 TMAX(5),ETAKMX(5),ETAMAX(5),PSIMAX(5),
3 EMMAX(5),FMAX(5),
4 RFMAX(5),PHIFMX(5),PHIMAX(5),WMAX(5)
COMMON /SPEC/WAV,XC(5),WC(5),WRC(5),XNAME(5),QFC(5),QDC(5),
1 QU2C(5),FLUXC(5),OMEGA(5),FLXU2C(5),URMSC(5)
COMMON /AMBIEN/ENA,UA,PSIA,PHIA,HA(3),WA(3),
1 UAX,UAY,UAZ,AA,BA,CA,RA,XA,YA,ZA,SHADOW
LOGICAL SHADOW
COMMON /NAGESH/PIK,UIK,UIKX,UIKY,UIKZ
ETAIK=0.
IF(SHADOW) GO TO 1
K=1
I=NS
CALL FAN(T,PSI,PHI)
IF(PSI.LT.PSIF-1.D-10) CALL SOF('PSI.LT.PSIF')
IF(PSI.GT.PSI1) PSI=PSI1
PSI0=PSI
CALL MATCH(T,PSI0,EM,TETA)
SPSI=DSIN(PSI)
CPSI=DCOS(PSI)
SPHI=DSIN(PHI)
CPHI=DCOS(PHI)
ST=DSIN(TETA)
CT=DCOS(TETA)
GOREM=1.D0+G1*EM**2
TERMN=GOREM**G6
U=EM*CO/DSQRT(GOREM)
UX=U*CT
UY=U*ST*CPHI
UZ=U*ST*SPHI
C COLLISION
MU1=WC(I)/(WC(I)+WA(K))
MU2=1.D0-MU1
UMX=MU1*UX+MU2*UAX
UMY=MU1*UY+MU2*UAY
UMZ=MU1*UZ+MU2*UAZ
DOTUM=OMEGX*UMX+OMEGY*UMY+OMEGZ*UMZ
URX=UX-UAX
URY=UY-UAY
URZ=UZ-UAZ
UR=DSQRT(URX**2+URY**2+URZ**2)
DET=DOTUM**2+(MU2*UR)**2-(UMX**2+UMY**2+UMZ**2)
IF(DET.LT.0.) GO TO 1
DET1=DSQRT(DET)
UIK1=-DOTUM+DET1
UIK2=-DOTUM-DET1

```

AMB0649
 AMB0650
 AMB0651
 AMB0652
 AMB0653
 AMB0654
 AMB0655
 AMB0656
 AMB0657
 AMB0658
 AMB0659
 AMB0660
 AMB0661
 AMB0662
 AMB0663
 AMB0664
 AMB0665
 AMB0666
 AMB0667
 AMB0668
 AMB0669
 AMB0670
 AMB0671
 AMB0672
 AMB0673
 AMB0674
 AMB0675
 AMB0676
 AMB0677
 AMB0678
 AMB0679
 AMB0680
 AMB0681
 AMB0682
 AMB0683
 AMB0684
 AMB0685
 AMB0686
 AMB0687
 AMB0688
 AMB0689
 AMB0690
 AMB0691
 AMB0692
 AMB0693
 AMB0694
 AMB0695
 AMB0696
 AMB0697
 AMB0698
 AMB0699
 AMB0700
 AMB0701
 AMB0702
 AMB0703
 AMB0704
 AMB0705
 AMB0706
 AMB0707
 AMB0708
 AMB0709
 AMB0710
 AMB0711
 AMB0712
 AMB0713
 AMB0714
 AMB0715
 AMB0716
 AMB0717
 AMB0718
 AMB0719
 AMB0720

```

IF(UIK2.GT.0.) CALL SOF('DOUBLE COLLISION OPTION NOT PROGRAMMED
1 YET')
UIK=UIK1
IF(UIK.LE.0.) GO TO 1
UIKX=-OMEGX*UIK
UIKY=-OMEGY*UIK
UIKZ=-OMEGZ*UIK
CDEL=(DOTUM+UIK)/(MU2*UR)
IF(CDEL.LE.0.) CALL SOF('CDEL NEGATIVE NOT PROGRAMMED YET')
IF(CDEL-1.D-10.GT.1.D0)
1 CALL SOF('CDEL (COS(DELTA)) CANNOT BE GT.1.')
PIK=(UIK/(MU2*UR))*2/(4.D0*PAI*CDEL)
IF (PIK.LT.0.) CALL SOF('PIK.LT.0')
FET=(UR/UA)*PIK/TERMN
UREL=DSQRT((UX-UIKX)**2+(UY-UIKY)**2+(UZ-UIKZ)**2)
GT=EL0*(UREL/UIK)/TERMN
CALL PATHIK(T,ETAIK)
POWER=ETAIK+ETAK-ALOGF
EFACT=0.
IF(POWER.LT.60.D0)EFACT=DEXP(-POWER)
FET=FET*EFACT
FETU2=FET*UIK**2
IF(EM.LT.0.) CALL SOF('EM.LT.0')
FETU2=FET*EM
RETURN
1 CONTINUE
FET=0.
FETU2=0.
GT=0.
RETURN
END
SUBROUTINE PATHIK(TC,ETAIK)
IMPLICIT REAL*8(A-H,O-Z)
REAL*8 MU1,MU2
COMMON /GAMA/G,G1,G2,G3,G4,G5,G6,G7,G8,G9,G10,G11,G12,G13,G14,G15,
1 G16,G17,G18,G19,G20
COMMON /PAR/CO,ENO,EM1,D,SIGMA,TLIM,DR0,EL0,Q0,T0,FACT,ALOGF,
1 DPSI0,DTMAX,DETA0,ETALIM,XSI,XSF
COMMON /NPAR/NPHI,IPAR,NP,NR,NX,NXS,NS,NSPEC,NS1,NS2,NTAU0,NETA0,
1 NAMB,NCASE,ICASE,IFAN
COMMON /GEOM/APF,PAI,PAI2,W,SW,CW,BETA,SBETA,CBETA,PSI1,SPSI1,
1 CPSI1,PSIF,SPSIF,CPSIF,TPS,F,AK,SK,CK,A0,RF,XF,YF,ZF,
2 PHISOF,PHIF,SPHIF,CPHIF,DYMIN,RMIN,XS,DIST,X0,Y0,Z0,
3 DY0,DEG,PSIN,ST1,CT1,OMEGX,OMEGY,OMEGZ,XSV(21)
COMMON /EPSIL/EPSETA,EPST,EPSR
COMMON /EXTREM/TEXT(5),ETAEXT(5),ETAKXT(5),PHIEXT(5),
1 PSIEXT(5),EMEXT(5),FEXT(5),WEXT(5),
2 TMAX(5),ETAKMX(5),ETAMAX(5),PSIMAX(5),
3 EMMAX(5),FMAX(5),
4 RFMAX(5),PHIFMX(5),PHIMAX(5),WMAX(5)
COMMON /SPEC/WAV,XC(5),WC(5),WRC(5),XNAME(5),QFC(5),QDC(5),
1 QU2C(5),FLUXC(5),OMEGA(5),FLXU2C(5),URMSC(5)
COMMON /AMBIEN/ENA,UA,PSIA,PHIA,HA(3),WA(3),
1 UAX,UAY,UAZ,AA,BA,CA,RA,XA,YA,ZA,SHADOW
LOGICAL SHADOW
NETA=NETA0
DT=TC/DBLE(NETA)
DT2=DT/2.D0
DT6=DT/6.D0
GT4=0.
T=0.
ETA=0.
IT=0
1 IT=IT+1
T1=T+DT2
T2=T+DT
GT1=GT4
CALL FT(T1,GT2)
GT3=GT2
CALL FT(T2,GT4)
DETA=DT6*(GT1+2.D0*(GT2+GT3)+GT4)
T=T+DT

```

```

ETA=ETA+DETA                                AMB0793
IF(IT.LT.NETA) GO TO 1                        AMB0794
ETAIK=ETA                                    AMB0795
RETURN                                        AMB0796
END                                            AMB0797
SUBROUTINE FT(T,GT)                           AMB0798
IMPLICIT REAL*8(A-H,O-Z)                     AMB0799
REAL*8 MU1,MU2                                AMB0800
COMMON /GAMA/G,G1,G2,G3,G4,G5,G6,G7,G8,G9,G10,G11,G12,G13,G14,G15, AMB0801
1      G16,G17,G18,G19,G20                    AMB0802
COMMON /PAR/C0,EN0,EM1,D,SIGMA,TLIM,DR0,EL0,Q0,T0,FACT,ALOGF, AMB0803
1      DPSI0,DTMAX,DETA0,ETALIM,XSI,XSF      AMB0804
COMMON /NPAR/NPHI,IPAR,NP,NR,NX,NXS,NS,NSPEC,NS1,NS2,NTAU0,NETA0, AMB0805
1      NAMB,NCASE,ICASE,IFAN                 AMB0806
COMMON /GEOM/APF,PAI,PAI2,W,SW,CW,BETA,SBETA,CBETA,PSI1,SPSI1, AMB0807
1      CPSI1,PSIF,SPSIF,CPSIF,TPSIF,AK,SK,CK,A0,RF,XF,YF,ZF, AMB0808
2      PHISO,PHIF,SPHIF,CPHIF,DYMIN,RMIN,XS,DIST,X0,Y0,Z0, AMB0809
3      DY0,DEG,PSIN,ST1,CT1,OMEGX,OMEGY,OMEGZ,XSV(21) AMB0810
COMMON /EPSIL/EPSETA,EPST,EPSR               AMB0811
COMMON /EXTREM/TEXT(5),ETAEXT(5),ETAKXT(5),PHIEXT(5), AMB0812
1      PSIEXT(5),EMEXT(5),FEXT(5),WEXT(5),    AMB0813
2      TMAX(5),ETAKMX(5),ETAMAX(5),PSIMAX(5), AMB0814
3      EMMAX(5),FMAX(5),                    AMB0815
4      RFMAX(5),PHIFMX(5),PHIMAX(5),WMAX(5)   AMB0816
COMMON /SPEC/WAV,XC(5),WC(5),WRC(5),XNAME(5),QFC(5),QDC(5), AMB0817
1      QU2C(5),FLUXC(5),OMEGA(5),FLXU2C(5),URMSC(5) AMB0818
COMMON /AMBIEN/ENA,UA,PSIA,PHIA,HA(3),WA(3), AMB0819
1      UAX,UAY,UAZ,AA,BA,CA,RA,XA,YA,ZA,SHADOW AMB0820
LOGICAL SHADOW                                AMB0821
COMMON /NAGESH/PIK,UIK,UIKX,UIKY,UIKZ       AMB0822
K=1                                            AMB0823
I=NS                                          AMB0824
CALL FAN(T,PSI,PHI)                           AMB0825
IF(PSI.LT.PSIF-1.D-10) CALL SOF('PSI.LT.PSIF') AMB0826
IF(PSI.GT.PSI1) PSI=PSI1                     AMB0827
PSI0=PSI                                       AMB0828
CALL MATCH(T,PSI0,EM,TETA)                   AMB0829
SPSI=DSIN(PSI)                                AMB0830
CPSI=DCOS(PSI)                                AMB0831
SPHI=DSIN(PHI)                                AMB0832
CPHI=DCOS(PHI)                                AMB0833
ST=DSIN(TETA)                                AMB0834
CT=DCOS(TETA)                                AMB0835
GOREM=1.D0+G1*EM**2                          AMB0836
TERMN=GOREM**G6                              AMB0837
U=EM*C0/DSQRT(GOREM)                         AMB0838
UX=U*CT                                       AMB0839
UY=U*ST*CPHI                                AMB0840
UZ=U*ST*SPHI                                AMB0841
UREL=DSQRT((UX-UIKX)**2+(UY-UIKY)**2+(UZ-UIKZ)**2) AMB0842
GT=EL0*(UREL/UIK)/TERMN                     AMB0843
RETURN                                        AMB0844
END                                            AMB0845
SUBROUTINE PATHK(T,ETAK)                      AMB0846
IMPLICIT REAL*8(A-H,O-Z)                     AMB0847
COMMON /GAMA/G,G1,G2,G3,G4,G5,G6,G7,G8,G9,G10,G11,G12,G13,G14,G15, AMB0848
1      G16,G17,G18,G19,G20                    AMB0849
COMMON /PAR/C0,EN0,EM1,D,SIGMA,TLIM,DR0,EL0,Q0,T0,FACT,ALOGF, AMB0850
1      DPSI0,DTMAX,DETA0,ETALIM,XSI,XSF      AMB0851
COMMON /NPAR/NPHI,IPAR,NP,NR,NX,NXS,NS,NSPEC,NS1,NS2,NTAU0,NETA0, AMB0852
1      NAMB,NCASE,ICASE,IFAN                 AMB0853
COMMON /GEOM/APF,PAI,PAI2,W,SW,CW,BETA,SBETA,CBETA,PSI1,SPSI1, AMB0854
1      CPSI1,PSIF,SPSIF,CPSIF,TPSIF,AK,SK,CK,A0,RF,XF,YF,ZF, AMB0855
2      PHISO,PHIF,SPHIF,CPHIF,DYMIN,RMIN,XS,DIST,X0,Y0,Z0, AMB0856
3      DY0,DEG,PSIN,ST1,CT1,OMEGX,OMEGY,OMEGZ,XSV(21) AMB0857
COMMON /EPSIL/EPSETA,EPST,EPSR               AMB0858
COMMON /EXTREM/TEXT(5),ETAEXT(5),ETAKXT(5),PHIEXT(5), AMB0859
1      PSIEXT(5),EMEXT(5),FEXT(5),WEXT(5),    AMB0860
2      TMAX(5),ETAKMX(5),ETAMAX(5),PSIMAX(5), AMB0861
3      EMMAX(5),FMAX(5),                    AMB0862
4      RFMAX(5),PHIFMX(5),PHIMAX(5),WMAX(5)   AMB0863
COMMON /COUNTS/ICONTC,ICONTT,ICNTOT,ICNTMX,IQTOT(5),ISHAD(5) AMB0864

```

```

COMMON /AMBIEN/ENA,UA,PSIA,PHIA,HA(3),WA(3),
1      UAX,UAY,UAZ,AA,BA,CA,RA,XA,YA,ZA,SHADOW
LOGICAL SHADOW
ETAK=0.
C DETERMINE POINT OF ENTRY OF AMBIENT TRAJECTORY TO FAN
TRF=TRF
XC=XF+TRF*OMEGX
YC=YF+TRF*OMEGY
ZC=ZF+TRF*OMEGZ
C CHECK SHADOW
SHADOW=.FALSE.
EVER=BA**2+CA**2
DETS=EVER*AO**2-(BA*ZC-CA*YC)**2
IF(DETS.LE.0.) GO TO 2
DETS1=DSQRT(DETS)
TAU1=(-(BA*YC+CA*ZC)+DETS1)/EVER
IF(TAU1.GT.0.) SHADOW=.TRUE.
2 CONTINUE
IF(SHADOW) GO TO 10
EVER1=AO+XC*TPSIF
EVER2=BA**2+CA**2-(AA*TPSIF)**2
EVER3=BA*YC+CA*ZC-AA*EVER1*TPSIF
DET=EVER3**2-EVER2*(YC**2+ZC**2-EVER1**2)
IF(DET.LE.0.)
1CALL SOF('NO INTERSECTION OF AMB. TRAJ. WITH LIMITING CONE')
DET1=DSQRT(DET)
TAUP=(-EVER3+DET1)/EVER2
TAUM=(-EVER3-DET1)/EVER2
IF(TAUP.GT.0. .AND. TAUM.GT.0.)
1CALL SOF('TWO POSITIVE INTERSECTIONS WITH LIMITING CONE.NOT PERMIT
1 IN THIS VERSION')
TAUF=DMAX1(TAUP,TAUM)
IF(TAUF.LE.0.)
1CALL SOF('NO POSITIVE INTERSECTION WITH LIMITING CONE')
XA=XC+TAUF*AA
YA=YC+TAUF*BA
ZA=ZC+TAUF*CA
RA=DSQRT(XA**2+(DSQRT(YA**2+ZA**2)-AO)**2)
TAUF=TAUF/RA
NTAU=NTAU0
DTAU=TAUF/DBLE(NTAU)
ETAK=0.
TAU=0.
DTAU2=DTAU/2.D0
DTAU6=DTAU/6.D0
GTAU4=0.
ITAU=0
1 ITAU=ITAU+1
TAU1=TAU+DTAU2
TAU2=TAU+DTAU
GTAU1=GTAU4
CALL FTAU(TAU1,GTAU2)
GTAU3=GTAU2
CALL FTAU(TAU2,GTAU4)
DETAU6=DTAU6*(GTAU1+2.D0*(GTAU2+GTAU3)+GTAU4)
TAU=TAU+DTAU
ETAK=ETAK+DETAU6
IF(ITAU.LT.NTAU) GO TO 1
ETAK=ETAK*(SIGMA*ENO*RA)
RETURN
10 CONTINUE
ISHAD(NS)=ISHAD(NS)+1
RETURN
END
SUBROUTINE FTAU(TAU,GTAU)
IMPLICIT REAL*8(A-H,O-Z)
COMMON /GAMA/G,G1,G2,G3,G4,G5,G6,G7,G8,G9,G10,G11,G12,G13,G14,G15,
1      G16,G17,G18,G19,G20
COMMON /PAR/CO,ENO,EM1,D,SIGMA,TLIM,DRO,ELO,Q0,T0,FACT,ALOGF,
1      DPSIO,DTMAX,DETA0,ETALIM,XSI,XSF
COMMON /NPAR/NPHI,IPAR,NP,NR,NX,NXS,NS,NSPEC,NS1,NS2,NTAU0,NETA0,
1      NAMB,NCASE,ICASE,IFAN

```

AMB0865
 AMB0866
 AMB0867
 AMB0868
 AMB0869
 AMB0870
 AMB0871
 AMB0872
 AMB0873
 AMB0874
 AMB0875
 AMB0876
 AMB0877
 AMB0878
 AMB0879
 AMB0880
 AMB0881
 AMB0882
 AMB0883
 AMB0884
 AMB0885
 AMB0886
 AMB0887
 AMB0888
 AMB0889
 AMB0890
 AMB0891
 AMB0892
 AMB0893
 AMB0894
 AMB0895
 AMB0896
 AMB0897
 AMB0898
 AMB0899
 AMB0900
 AMB0901
 AMB0902
 AMB0903
 AMB0904
 AMB0905
 AMB0906
 AMB0907
 AMB0908
 AMB0909
 AMB0910
 AMB0911
 AMB0912
 AMB0913
 AMB0914
 AMB0915
 AMB0916
 AMB0917
 AMB0918
 AMB0919
 AMB0920
 AMB0921
 AMB0922
 AMB0923
 AMB0924
 AMB0925
 AMB0926
 AMB0927
 AMB0928
 AMB0929
 AMB0930
 AMB0931
 AMB0932
 AMB0933
 AMB0934
 AMB0935
 AMB0936


```

COMMON /GEOM/APF,PAI,PAI2,W,SW,CW,BETA,SBETA,CBETA,PSI1,SPSI1,      AMB0937
1      CPSI1,PSIF,SPSIF,CPSIF,TPSIF,AK,SK,CK,A0,RF,XF,YF,ZF,      AMB0938
2      PHISOF,PHIF,SPHIF,CPHIF,DYMIN,RMIN,XS,DIST,X0,Y0,Z0,      AMB0939
3      DY0,DEG,PSIN,ST1,CT1,OMEGX,OMEGY,OMEGZ,XSV(21)      AMB0940
COMMON /EPSIL/EPSETA,EPST,EPSR      AMB0941
COMMON /EXTREM/TEXT(5),ETAEXT(5),ETAKXT(5),PHIEXT(5),      AMB0942
1      PSIEXT(5),EMEXT(5),FEXT(5),WEXT(5),      AMB0943
2      TMAX(5),ETAKMX(5),ETAMAX(5),PSIMAX(5),      AMB0944
3      EMMAX(5),FMAX(5),      AMB0945
4      RFMAX(5),PHIFMX(5),PHIMAX(5),WMAX(5)      AMB0946
COMMON /SPEC/WAV,XC(5),WC(5),WRC(5),XNAME(5),QFC(5),QDC(5),      AMB0947
1      QU2C(5),FLUXC(5),OMEGA(5),FLXU2C(5),URMSC(5)      AMB0948
COMMON /AMBIEN/ENA,UA,PSIA,PHIA,HA(3),WA(3),      AMB0949
1      UAX,UAY,UAZ,AA,BA,CA,RA,XA,YA,ZA,SHADOW      AMB0950
LOGICAL SHADOW      AMB0951
CALL FANT(TAU,PSI,PHI)      AMB0952
IF(PSI.LT.PSIF-1.D-10) CALL SOF('PSI.LT.PSIF')      AMB0953
IF(PSI.GT.PSI1) PSI=PSI1      AMB0954
PSI0=PSI      AMB0955
CALL MATCH(T,PSI0,EM,TETA)      AMB0956
SPSI=DSIN(PSI)      AMB0957
CPSI=DCOS(PSI)      AMB0958
SPHI=DSIN(PHI)      AMB0959
CPHI=DCOS(PHI)      AMB0960
ST=DSIN(TETA)      AMB0961
CT=DCOS(TETA)      AMB0962
GOREM=1.D+G1*EM**2      AMB0963
TERMN=GOREM**G6      AMB0964
U=EM*CO/DSQRT(GOREM)      AMB0965
UREL=DSQRT((CT*U-UAX)**2+(ST*CPHI*U-UAY)**2+(ST*SPHI*U-UAZ)**2)      AMB0966
GTAU=UREL/(UA*TERMN)      AMB0967
RETURN      AMB0968
END      AMB0969
SUBROUTINE FAN(T,PSI,PHI)      AMB0970
IMPLICIT REAL*8(A-H,O-Z)      AMB0971
COMMON /PAR/CO,ENO,EM1,D,SIGMA,TLIM,DR0,ELO,Q0,T0,FACT,ALOGF,      AMB0972
1      DPSI0,DTMAX,DETA0,ETALIM,XSI,XSF      AMB0973
COMMON /GEOM/APF,PAI,PAI2,W,SW,CW,BETA,SBETA,CBETA,PSI1,SPSI1,      AMB0974
1      CPSI1,PSIF,SPSIF,CPSIF,TPSIF,AK,SK,CK,A0,RF,XF,YF,ZF,      AMB0975
2      PHISOF,PHIF,SPHIF,CPHIF,DYMIN,RMIN,XS,DIST,X0,Y0,Z0,      AMB0976
3      DY0,DEG,PSIN,ST1,CT1,OMEGX,OMEGY,OMEGZ,XSV(21)      AMB0977
COMMON /POINT/XP,YP,XCOR,YCOR      AMB0978
C RING FAN GEOMETRY. FAN CORNER IS AT (0,A0*COS(PHI),A0*SIN(PHI)).      AMB0979
C RF -- RADIAL DISTANCE ON LIMITING CHARACTERISTIC OF POINT OF      AMB0980
C ENTRANCE OF RAY.      AMB0981
C DIRECTION COSINES OF RAY: OMEGX,OMEGY,OMEGZ      AMB0982
TRF=T*RF      AMB0983
X=XF+TRF*OMEGX      AMB0984
Y=YF+TRF*OMEGY      AMB0985
Z=ZF+TRF*OMEGZ      AMB0986
DY=DSQRT(Y*Y+Z*Z)-A0      AMB0987
IF(DABS(DY).LE.1.D-10*A0) DY=1.D-10*A0      AMB0988
IF(DY.LT.0.)      AMB0989
1CALL SOF('POINT X,Y,X CANNOT BE CLOSER TO X-AXIS THAN RADIUS A0')      AMB0990
YY=X/DY      AMB0991
PSI=PAI2-DATAN(YY)      AMB0992
PHI=DATAN(Z/Y)      AMB0993
XP=XCOR+X      AMB0994
YP=A0+DY      AMB0995
RETURN      AMB0996
END      AMB0997
SUBROUTINE FANT(TAU,PSI,PHI)      AMB0998
IMPLICIT REAL*8(A-H,O-Z)      AMB0999
COMMON /PAR/CO,ENO,EM1,D,SIGMA,TLIM,DR0,ELO,Q0,T0,FACT,ALOGF,      AMB1000
1      DPSI0,DTMAX,DETA0,ETALIM,XSI,XSF      AMB1001
COMMON /GEOM/APF,PAI,PAI2,W,SW,CW,BETA,SBETA,CBETA,PSI1,SPSI1,      AMB1002
1      CPSI1,PSIF,SPSIF,CPSIF,TPSIF,AK,SK,CK,A0,RF,XF,YF,ZF,      AMB1003
2      PHISOF,PHIF,SPHIF,CPHIF,DYMIN,RMIN,XS,DIST,X0,Y0,Z0,      AMB1004
3      DY0,DEG,PSIN,ST1,CT1,OMEGX,OMEGY,OMEGZ,XSV(21)      AMB1005
COMMON /AMBIEN/ENA,UA,PSIA,PHIA,HA(3),WA(3),      AMB1006
1      UAX,UAY,UAZ,AA,BA,CA,RA,XA,YA,ZA,SHADOW      AMB1007
COMMON /POINT/XP,YP,XCOR,YCOR      AMB1008

```

```

LOGICAL SHADOW
C RING FAN GEOMETRY. FAN CORNER IS AT (0,A0*COS(PHI),A0*SIN(PHI)).
C RA -- RADIAL DISTANCE ON LIMITING CHARACTERISTIC OF POINT OF
C ENTRANCE OF RAY.
C DIRECTION COSINES OF RAY: -AA,-BA,-CA
TRA=TAU*RA
X=XA-TRA*AA
Y=YA-TRA*BA
Z=ZA-TRA*CA
DY=DSQRT(Y*Y+Z*Z)-A0
IF(DABS(DY).LE.1.D-10*A0) DY=1.D-10*A0
IF(DY.LT.0.)
1CALL SOF('POINT X,Y,X CANNOT BE CLOSER TO X-AXIS THAN RADIUS A0')
YY=X/DY
PSI=PAI2-DATAN(YY)
PHI=DATAN(Z/Y)
XP=XCOR+X
YP=A0+DY
RETURN
END
SUBROUTINE HMSET
C SUBROUTINE NUMBER 20
IMPLICIT REAL*8(A-H,O-Z,$)
REAL*8 KAPAOB,MHINV,MINVO,M,MF,M1,M2,M3,NORM,MEXIT,LAMD0B
COMMON /GAMA/G,G1,G2,G3,G4,G5,G6,G7,G8,G9,G10,G11,G12,G13,G14,G15,
1 G16,G17,G18,G19,G20
COMMON /PAR/CO,ENO,EM1,D,SIGMA,TLIM,DRO,ELO,QO,TO,FACT,ALOGF,
1 DPSIO,DTMAX,DETA0,ETALIM,XSI,XSF
COMMON /GEOM/APF,PAI,PAI2,W,SW,CW,BETA,SBETA,CBETA,PSI1,SPSI1,
1 CPSI1,PSIF,SPSIF,CPSIF,TPSIF,AK,SK,CK,A0,RF,XF,YF,ZF,
2 PHISO,PHIF,SPHIF,CPHIF,DYMIN,RMIN,XS,DIST,X0,Y0,Z0,
3 DY0,DEG,PSIN,ST1,CT1,OMEGX,OMEGY,OMEGZ,XSV(21)
COMMON /GRP/DMINV,MHINV(101),HNV(101)
COMMON /IGRP/KHM
C A ROUTINE FOR THE C+ DERIVATIVE DUE TO RING SYMMETRY (GRP).
MEXIT=EM1
KHM=51
IF(KHM.GT.101) CALL SOF('2001')
MINVO=1.D0/MEXIT
DMINV=MINVO/DBLE(KHM-1)
M=MEXIT
SUM=0.
KHM1=KHM-1
DO 1 I=1,KHM1
MF=M
MHINV(I)=MINVO-DBLE(I-1)*DMINV
M=1.D0/MHINV(I)
DM=M-MF
M1=M-DM
M2=M-DM/2.D0
M3=M
CALL MFUNC(M1,F1,ETALF1,TETA1)
CALL MFUNC(M2,F2,ETALF2,TETA2)
CALL MFUNC(M3,F3,ETALF3,TETA3)
SUM=SUM+DM*(F1+4.D0*F2+F3)/6.D0
ETALF=ETALF3
TETA=TETA3
PSI=TETA+DASIN(1.D0/M)
NORM=((3.D0-G)/4.D0)*(M**2-1.D0)**0.75D0/
1 (DSIN(PSI)*(1.D0+G1*M**2)**G14)
HM=SUM*NORM
HNV(I)=HM
GOREM=1.D0+G1*M**2
GOR=M**2-1.D0
DELTOB=0.5D0*DSQRT(GOR)*(1.D0/(MEXIT*ETALF)
1 +DSIN(TETA)/M)/DSIN(PSI)+G15*HM/2.D0
EPSIOB=DELTOB/DSQRT(GOR)-DSIN(TETA)/(M*DSIN(PSI))
KAPAOB=1.D0
IF(DABS(PAI2-TETA).GT.1.D-6)
1KAPAOB=DTAN(TETA)*EPSIOB
LAMD0B=EPSIOB-DELTOB*GOREM/(GOR*DSQRT(GOR))
PRINT 11,I,M,HM,TETA*DEG,PSI*DEG

```

```

11  FORMAT(/1X, '          I,M,MM,TETA,PSI=',I5,5D12.4)          AMB1081
    PRINT 12,DELTOB,EPSIOB*DEG,KAPAOB*DEG,LAMDOB*DEG          AMB1082
12  FORMAT( 1X,'DELTOB,EPSIOB,KAPAOB,LAMDOB=',5X,5D12.4)      AMB1083
1   CONTINUE          AMB1084
    MHINV(KHM)=0.      AMB1085
    HMOV(KHM)=1.D0     AMB1086
    RETURN            AMB1087
    END              AMB1088
    SUBROUTINE MFUNC(M,F,ETALF,TETA)          AMB1089
C  SUBROUTINE NUMBER 21          AMB1090
    IMPLICIT REAL*8(A-H,O-Z,$)              AMB1091
    REAL*8 NU,NUFUNC,M,MEXIT,MD,MDD          AMB1092
    COMMON /GAMA/G,G1,G2,G3,G4,G5,G6,G7,G8,G9,G10,G11,G12,G13,G14,G15, AMB1093
1   G16,G17,G18,G19,G20                      AMB1094
    COMMON /PAR/CO,ENO,EM1,D,SIGMA,TLIM,DR0,EL0,Q0,T0,FACT,ALOGF, AMB1095
1   DPSIO,DTMAX,DETA0,ETALIM,XSI,XSF        AMB1096
    COMMON /GEOM/APF,PAI,PAI2,W,SW,CW,BETA,SBETA,CBETA,PSI1,SPSI1, AMB1097
1   CPSI1,PSIF,SPSIF,CPSIF,TPSIF,AK,SK,CK,A0,RF,XF,YF,ZF, AMB1098
2   PHISOF,PHIF,SPHIF,CPHIF,DYMIN,RMIN,XS,DIST,X0,Y0,Z0, AMB1099
3   DY0,DEG,PSIN,ST1,CT1,OMEGX,OMEGY,OMEGZ,XSV(21) AMB1100
C                                          AMB1101
    QF(MDD)=1.D0/DSQRT(MDD**2-1.D0)          AMB1102
C                                          AMB1103
    NUFUNC(MD)=-G5*DATAN(G5*QF(MD))+DATAN(QF(MD)) AMB1104
C                                          AMB1105
    MEXIT=EM1                                AMB1106
    NU=NUFUNC(M)                             AMB1107
    TETA=NUFUNC(MEXIT)+PAI2-NU               AMB1108
    GOREM=1.D0+G1*M**2                       AMB1109
    GOR=M**2-1.D0                            AMB1110
    F=(M**2)*(GOREM**G13)*DSIN(TETA)/GOR**1.25D0 AMB1111
    GOREM1=1.D0+G1*MEXIT**2                 AMB1112
    GOR1=MEXIT**2-1.D0                      AMB1113
    ETALF=((GOREM/GOREM1)**G14)*((GOR1/GOR)**0.25D0) AMB1114
    RETURN                                  AMB1115
    END                                    AMB1116
    SUBROUTINE HINTER(M,H)                  AMB1117
C  SUBROUTINE NUMBER 22                  AMB1118
    IMPLICIT REAL*8(A-H,O-Z,$)              AMB1119
    REAL*8 MINV,M,MEXIT,MHINV              AMB1120
    COMMON /GAMA/G,G1,G2,G3,G4,G5,G6,G7,G8,G9,G10,G11,G12,G13,G14,G15, AMB1121
1   G16,G17,G18,G19,G20                      AMB1122
    COMMON /PAR/CO,ENO,EM1,D,SIGMA,TLIM,DR0,EL0,Q0,T0,FACT,ALOGF, AMB1123
1   DPSIO,DTMAX,DETA0,ETALIM,XSI,XSF        AMB1124
    COMMON /GRP/DMINV,MHINV(101),HMOV(101)   AMB1125
    COMMON /IGRP/KHM                        AMB1126
C  COMPUTE H(M) BY INTERPOLATION          AMB1127
    MEXIT=EM1                                AMB1128
    MINV=1.D0/M                             AMB1129
    I=KHM-IDINT(MINV/DMINV-1.D-9)-1         AMB1130
    IF(I.GE.1.AND.I.LT.KHM) GO TO 1         AMB1131
    PRINT 11,I,KHM,M,MEXIT                  AMB1132
11  FORMAT(/1X,'I,KHM,M,MEXIT=',2I5,2D14.6/) AMB1133
    CALL SOF('2201')                        AMB1134
1   CONTINUE                                AMB1135
    F1=(MINV-MHINV(I+1))/DMINV              AMB1136
    F2=1.D0-F1                             AMB1137
    IF(F1.LT.-1.D-9) CALL SOF('2210')       AMB1138
    IF(F2.LT.-1.D-9) CALL SOF('2211')       AMB1139
    H=F1*HMOV(I)+F2*HMOV(I+1)              AMB1140
    RETURN                                  AMB1141
    END                                    AMB1142
    SUBROUTINE MATCH(T,PSIO,MAB,TETAAB)     AMB1143
C  SUBROUTINE NUMBER 23                  AMB1144
    IMPLICIT REAL*8(A-H,O-Z,$)              AMB1145
    REAL*8 M,M0B,MEXIT,MAB,LAMDOB,KAPAOB   AMB1146
    COMMON /GAMA/G,G1,G2,G3,G4,G5,G6,G7,G8,G9,G10,G11,G12,G13,G14,G15, AMB1147
1   G16,G17,G18,G19,G20                      AMB1148
    COMMON /PAR/CO,ENO,EM1,D,SIGMA,TLIM,DR0,EL0,Q0,T0,FACT,ALOGF, AMB1149
1   DPSIO,DTMAX,DETA0,ETALIM,XSI,XSF        AMB1150
    COMMON /NPAR/NPHI,IPAR,NP,NR,NX,NXS,NS,NSPEC,NS1,NS2,NTAU0,NETA0, AMB1151
1   NAMB,NCASE,ICASE,IFAN                  AMB1152
    COMMON /GEOM/APF,PAI,PAI2,W,SW,CW,BETA,SBETA,CBETA,PSI1,SPSI1,

```

```

1      CPSI1,PSIF,SPSIF,CPSIF,TPSIF,AK,SK,CK,A0,RF,XF,YF,ZF,AMB1153
2      PHISO,PHIF,SPHIF,CPHIF,DYMIN,RMIN,XS,DIST,X0,Y0,Z0,AMB1154
3      DY0,DEG,PSIN,ST1,CT1,OMEGX,OMEGY,OMEGZ,XSV(21)AMB1155
COMMON /POINT/XP,YP,XCOR,YCORAMB1156
COMMON /GRP/DMINV,MHINV(101),HNV(101)AMB1157
COMMON /IGRP/KHMAMB1158
MEXIT=EM1AMB1159
GO TO (101,102),IFANAMB1160
101  CONTINUEAMB1161
C  FAN APPROXIMATED AS PLANARAMB1162
MAB=DSQRT(1.D0+G4/DTAN((PSI-PSIF)/G5)**2)AMB1163
TETAAB=PSI0-DASIN(1.D0/MAB)AMB1164
GO TO 100AMB1165
102  CONTINUEAMB1166
C  COMPUTE MAB FROM THE INVERSE PROBLEM SOLUTIONAMB1167
COTAV=1.D0/DTAN(PSI0)AMB1168
EVY=YP*DLOG(YP/YCOR)/(YP-YCOR)-1.D0AMB1169
PSIN=PSI0AMB1170
DO 1 ITER=1,10AMB1171
PSI=PSINAMB1172
M=DSQRT(1.D0+G4/DTAN((PSI-PSIF)/G5)**2)AMB1173
M=DMAX1(M,MEXIT)AMB1174
CALL HINTER(M,HM)AMB1175
CALL MFUNC(M,F,ETALF,TETA)AMB1176
GOREM=1.D0+G1*M**2AMB1177
GOR=M**2-1.D0AMB1178
DELTOB=0.5D0*DSQRT(GOR)*(1.D0/(MEXIT*ETALF)AMB1179
+DSIN(TETA)/M)/DSIN(PSI)+G15*HM/2.D0AMB1180
EPSIOB=DELTOB/DSQRT(GOR)-DSIN(TETA)/(M*DSIN(PSI))AMB1181
LAMDOB=EPSIOB-DELTOB*GOREM/(GOR*DSQRT(GOR))AMB1182
COTN=COTAV+LAMDOB*EVY/DSIN(PSI)**2AMB1183
PSIN=PAI2-DATAN(COTN)AMB1184
DPSI=PSIN-PSIAMB1185
IF(DABS(DPSI).LT.1.D-6) GO TO 11AMB1186
1  CONTINUEAMB1187
PRINT 12,I,ITER,PSI,PSIN,DPSI,M,XP,YP,TAMB1188
12  FORMAT(/IX,'I,ITER,PSI,PSIN,DPSI,M,XP,YP,T='//AMB1189
1  1X,2I4,7D11.3/)AMB1190
CALL SQ('2301')AMB1191
11  CONTINUEAMB1192
C  USING MOB=M AS COMPUTED FROM THE INVERSE PROBLEM, FIND MAB.AMB1193
MOB=MAMB1194
CALL MFUNC(M,F,ETALF,TETA)AMB1195
PSI=TETA+DASIN(1.D0/M)AMB1196
CALL HINTER(M,HM)AMB1197
GOREM=1.D0+G1*M**2AMB1198
GOR=M**2-1.D0AMB1199
DELTOB=0.5D0*DSQRT(GOR)*(1.D0/(MEXIT*ETALF)AMB1200
+DSIN(TETA)/M)/DSIN(PSI)+G15*HM/2.D0AMB1201
FOB=(G7*GOREM)**G2/MAMB1202
FAB=FOB*(YP/YCOR)**DELTOBAMB1203
CALL AREA(FAB,MAB)AMB1204
EPSIOB=DELTOB/DSQRT(GOR)-DSIN(TETA)/(M*DSIN(PSI))AMB1205
KAPAOB=1.D0AMB1206
IF(DABS(PAI2-TETA).GT.1.D-8)AMB1207
1KAPAOB=DTAN(TETA)*EPSIOBAMB1208
COSTAB=DCOS(TETA)*(YP/YCOR)*(-KAPAOB)AMB1209
TETAAB=DACOS(COSTAB)AMB1210
100  CONTINUEAMB1211
RETURNAMB1212
ENDAMB1213
SUBROUTINE AREA(F,M)AMB1214
C  SUBROUTINE NUMBER 24AMB1215
IMPLICIT REAL*8(A-H,O-Z,$)AMB1216
REAL*8 MEXIT,MIN,M,MHINVAMB1217
COMMON /GAMA/G,G1,G2,G3,G4,G5,G6,G7,G8,G9,G10,G11,G12,G13,G14,G15,AMB1218
G16,G17,G18,G19,G20AMB1219
COMMON /PAR/CO,ENO,EM1,D,SIGMA,TIM,DR0,EL0,Q0,T0,FACT,ALOGF,AMB1220
DPSI0,DTMAX,DETA0,ETALIM,XSI,XSFAMB1221
COMMON /GRP/DMINV,MHINV(101),HNV(101)AMB1222
COMMON /IGRP/KHMAMB1223
C  COMPUTE MACH NUMBER M FROM AREA RATIO FUNCTION FAMB1224

```

C	F=((2/(G+1))*(1+(G-1)*M**2))*((G+1)/(2*(G-1)))/M	AMB1225
C	INITIAL GUESS IS MIN	AMB1226
	MEXIT=EM1	AMB1227
	E1=(F*MEXIT)**(1.D0/G2)/G7	AMB1228
	E2=(E1-1.D0)/G1	AMB1229
	E3=DMAX1(E2,MEXIT**2)	AMB1230
	MIN=DSQRT(E3)	AMB1231
	EMN=MIN	AMB1232
	DO 1 I=1,100	AMB1233
	EMO=EMN	AMB1234
	GOREM=1.D0+G1*EMO**2	AMB1235
	GOR=EMO**2-1.D0	AMB1236
	FO=(C7*GOREM)**G2/EMO	AMB1237
	DF=FO-F	AMB1238
C	PRINT 123,I,EMO,EMN,FO,F,DF,GOR,GOREM	AMB1239
C123	FORMAT(1X,'I,EMO,EMN,FO,F,DF,GOR,GOREM=',I5,7D12.4)	AMB1240
	DFDM=FO*GOR/(EMO*GOREM)	AMB1241
	DMN=DF/DFDM	AMB1242
	EMN=EMO-DMN	AMB1243
	EPSEM=DABS(DMN/EMN)	AMB1244
	IF(EPSEM.LT.1.D-10) GO TO 11	AMB1245
1	CONTINUE	AMB1246
	CALL SQF('2401')	AMB1247
11	CONTINUE	AMB1248
	M=EMN	AMB1249
	RETURN	AMB1250
	END	AMB1251

8. DISTRIBUTION LIST

No. of Copies

1. Defense Technical Information Center
Cameron Station
Alexandria, VA 22314 2
2. Library, Code 0142
Naval Postgraduate School
Monterey, CA 93943-5100. 2
3. Department Chairman, Code 67
Department of Aeronautics
Naval Postgraduate School
Monterey, CA 93943-5100. 1
4. Distinguished Professor Allen E. Fuhs
Space Systems Academic Group, Code 72
Naval Postgraduate School
Monterey, CA 93943-5100. 5
5. Dr. Neil Griff
SDIO DEO
Washington, DC 20301-7100. 3
6. Mr. Bruce Pierce
SDIO DEO
Washington, DC 20301-7100. 1
7. Dr. Joseph Falcovitz (24)
Rafael Ballistic Center
P. O. Box 2250 , Haifa
Israel 5

8. Professor Oscar Biblarz
 Department of Aeronautics, Code 67
 Naval Postgraduate School
 Monterey, CA 93943-5100. 1

9. Research Administration Office
 Code 012
 Naval Postgraduate School
 Monterey, CA 93943-5100. 1

10. Dr. P. Avizonis
 Air Force Weapons Laboratory
 Kirtland Air Force Base, NM 87117 1

11. Dr. John Lawless
 Space Power Inc.
 1977 Concourse Drive
 San Jose, CA 95131 1

12. Dr. Mark Thornton
 Boeing Aerospace Company
 Post Office Box 3999
 Seattle, WA 98124-2499 1

13. LT. Mark Price
 AFRPL
 Edwards AFB, CA 93523 1

14. Mr. Arthur W. Rogers
 Space Systems Division
 Hughes Aircraft Co.
 P. O. Box 92919, Los Angeles, CA 90009 1

15. LCOL Rick Babcock, USAF
Air Force Geophysical Laboratory
Hanscomb Field
Bedford, MA 01730 1

16. Mr. Ronald J. Hoffman
Plume Technology and Spacecraft
Contamination Division
Science Applications International Co.
10000 Santa Monica Blvd., Suite 320
Los Angeles, CA 90067 1

END

9-87

Dtic